Title:

Ipsilateral restriction of chromosome movement along a centrosome, and apical-basal axis during the cell cycle

Authors and Affiliations:

Pingping Cai*[,1], Christian J. Casas*[,2], Lisa L. Hua[2], and Takashi Mikawa[1]
*Equal contribution
[1]Cardiovascular Research Institute, University of California, San Francisco
[2]Department of Biology, Sonoma State University
Co-corresponding authors: takashi.mikawa@ucsf.edu, hual@sonoma.edu

Abstract:

Individual homologous chromosomes are spatially segregated into haploid chromosome sets along the centrosome axis in an antipairing configuration. Disruption of the antipairing pattern occurs in cancer cells. However, little is known about how this spatial organization of chromosomes is established or maintained. Here, we report that there is a zone of diminished interchromosomal linkage and centromere components between haploid sets in primary and established human epithelial cell lines. Using 4-Dimensional live cell imaging analysis of centromere and centrosome tracking, we show ipsilateral restriction of chromosome oscillations along the diminished zone, coincident with the centrosome and apical-basal axis from mitosis onset to G1 interphase. We propose a biophysical model of axis-dependent ipsilateral restriction of chromosome oscillations for haploid set organization.

Keywords:

homologous chromosomes, nuclear organization, antipairing, haploid set segregation, interchromosomal linkages, centromere dynamics, satellite sequences, CENP-A, CENP-B, centrin1

Introduction:

Chromosomes are highly organized structures within the nucleus of the cell (Cooper, 2000). Multiple studies have investigated the distribution of chromosomes across various human cell types, and have proposed different models for individual chromosome organization (reviewed in Hua et al., 2022). Interphase chromosome organization is radially distributed in the nucleus in what was originally thought to be random patterns (Emmerich et al., 1989; Lesko et al., 1995), but is increasingly correlated with factors such as chromosome size, gene density, or heterochromatic content (Cremer et al., 2001; Bolzer et al., 2005; Bridger et al., 2000; Boyle et al., 2001; Küpper et al., 2007). Variations across different cell types (Parada et. al, 2004), and nuclear morphologies (Neusser et al., 2007) have also complicated the interpretation for one consistent model for chromosome organization in human cells. For example, previous studies at

interphase, and mitosis have reported that larger chromosomes are positioned towards the periphery, while smaller chromosomes are positioned to the center of the nucleus (Sun et al., 2000; Mosgöller et al., 1991). Although chromosomes 18 and 19 are similar in size, they differ in gene density. Croft et al. (1999) and Cremer et al. (2001) found that gene-poor chromosome 18, and gene-rich chromosome 19, localize to peripheral, and central regions of the nucleus, respectively. They propose that gene density determines chromosome positioning rather than chromosome size (Croft et al., 1999; Cremer et al., 2001). Cell types with different nuclear morphologies and different fixation techniques have also been proposed, contributing to these conflicting studies (Mayer et al., 2005; Alcobia et al., 2000; Kim et al., 2004; Marella et al., 2009).

We have previously demonstrated the presence of a haploid (1n) chromosome set organization in primary human umbilical vein endothelial cells (HUVECs) (Hua and Mikawa, 2018). We found that all homologous autosomal pairs, and the sex chromosomes were segregated, or antipaired, across the centrosome axis at metaphase/early anaphase in HUVECs (Hua and Mikawa, 2018). This segregation pattern defined a haploid chromosome set (1n) per nuclear hemisphere organization, as defined by the centrosome axis, and was shown to be consistent across multiple cell types (Hua and Mikawa, 2018). However, how the individual chromosomes within a haploid set remain together, and are excluded from the other haploid set is unknown.

Multiple mechanisms for this segregation pattern may exist, and they may not be mutually exclusive from each other. One potential mechanism could be DNA-based interchromosomal linkages between individual chromosomes within each haploid set that may physically tether the chromosomes together. Additionally, the haploid sets may be defined by parental origin, or there may be epigenetic differences between the two haploid sets that the cell recognizes for their spatial segregation. A mechanism of physical compartmentalization of haploid sets by molecular cages, or cytoskeletal elements, could also prevent chromosomes of different sets from mixing together.

Here, we investigate the organization of interchromosomal linkage components *in vivo*. Early studies using electron microscopy, and Giemsa staining of metaphase spread chromosomes first described the existence of interchromosomal linkages in human, mouse, and Chinese Hamster cells (Emmerich et al., 1973; Jaffray and Geneix, 1974; Takayama, 1975; Burdick, 1976). These interchromosomal linkages were shown to stain positive with Hoechst DNA dye (Maniotis et al., 1997). Subsequent micromanipulation experiments demonstrated that chromosomes moved in concert when pulled under tension, and could be mechanically dissected together as “beads on a string” in human cell lines (Maniotis et al., 1997; Marko, 2008). DNA-based linkages were also corroborated by DNA Fluorescence in situ hybridization (FISH) assays in metaphase spread preparations of human and mouse cells (Kuznetsova et al., 2007; Potapova et al., 2019).

Linkages between individual chromosomes have been shown to stain positive for sequences found within the peri/centromeric DNA regions of the chromosomes (Saifitdinova et al., 2001; Kuznetsova et al., 2007; Potapova et al., 2019). These regions are typically condensed as

heterochromatin, low in gene density, and rich in tandem DNA satellite repeats (Jagannathan and Yamashita, 2017; Bloom, 2014; Pidoux and Allshire, 2005; Guenatri et al., 2004; Saksouk et al., 2015; Jones, 1970; Jones, 1973; Wijchers et al., 2015). In mice, Jagannathan et al. (2018) showed linkages that stained positive for a major centromeric DNA satellite sequence in mitotic cells. Although the presence of these interchromosomal linkages have been reported, their function in the cell remains unknown.

In this study, we characterize the components of interchromosomal linkages within intact human mitotic cells. Past studies utilized metaphase spreads, which may damage the 3D endogenous spatial organization of chromosomes, and linkage structures (Saifitdinova et al., 2001; Kuznetsova et al., 2007; Potapova et al., 2019). Our study aims to investigate the organization of interchromosomal linkage components *in situ* in primary cells.

Using fixed and live cell marker analysis, we find a diminished zone devoid of these linkage components along the centrosome axis between the chromosome sets in metaphase cells. Using 4D time lapse microscopy, centromere movements were found to be restricted in an ipsilateral axis-dependent manner. The centromere positions are largely restricted from mitosis onset to G1 interphase, even as the mitotic spindle is assembling, and disassembling. This suggests other non-spindle regulatory mechanisms, such as a diminished zone and/or interchromosomal linkages that may maintain individual chromosome positions throughout the cell cycle. This previously unrecognized ipsilateral-based restriction of chromosome organization and dynamics may contribute to haploid chromosome set segregation.

Results:

Characterization of interchromosomal linkage components of DNA satellite sequences, and the CENP-B protein

To test whether interchromosomal linkages are present in HUVECs *in vivo*, we conducted a survey of cells throughout mitosis, examining the organization of DNA α-satellite and cenpb sequences (Figure 1A-C). HUVECs were used to identify the haploid chromosome set-based, or antipairing, organization along the centrosome axis in metaphase/early anaphase cells (Hua and Mikawa, 2018) (Figure 1–figure supplement 1). HUVECs are adherent primary endothelial cells that demonstrate apical/basal polarity when grown in culture (Muller and Gimbrone, 1986); thus, we were able to establish an axial coordinate system using the centrosomes as subcellular markers to define the x-axis; the optical path to define the z-axis; and the line perpendicular to both the x-, and z-axes to define the y-axis. (Hua and Mikawa, 2018) (Figure 1P). Visualization of the centrosomes by γ-tubulin IF was also used for accurate staging for each mitotic cell, and allowed for indirect identification of the haploid chromosome sets across the centrosome axis at metaphase.

Throughout mitosis, interchromosomal linkage components were clearly identified at metaphase (Figure 1B). Interconnected satellite staining, indicative of centromeric associations, were visible between foci within the DNA mass. The centromeric associations were not obvious at

prometaphase and anaphase (Figure 1A, C), however, due to chromosome compaction (Magidson et al., 2011; Itoh et al., 2018; Mora-Bermúdez et al., 2007). Therefore, HUVECs at metaphase were used for linkage characterization and analysis. At metaphase, individual channels for α-satellite (Figure 1D) and cenpb sequences (Figure 1E) also revealed a diminished zone of DNA satellite staining (n=23/33). This interchromosomal linkage diminished zone (IcL-DZ) was on average 0.77 μm +/- 0.19 μm s.d. in width, and persisted across the metaphase DNA mass. In contrast, aggregates of centromeric associations were observed on either side of the IcL-DZ (Figure 1D-E).

To test whether an interchromosomal linkage diminished zone (IcL-DZ) is conserved across multiple HUVECs at metaphase, we constructed a comprehensive heatmap of the DNA satellite staining by aligning individual cells along their centrosome axis using the axial coordinate system as defined by Hua and Mikawa (2018) (Figure 1P). The heatmap provides objective quantification of the signal to noise intensity for the IcL-DZ, as gaps are present between centromere foci throughout the metaphase mass. However, individual centromeres can oscillate at a range of ~2 μm min^{-1} during metaphase in live cells (Walczak et al., 2010) and may mask the IcL-DZ from a top view perspective. Therefore, to test this possibility, we applied a rotational analysis for each cell along different axes to determine if an IcL-DZ could be identified (figure Figure 1–figure supplement 2). We found a consistent IcL-DZ following an average of ~18° rotation along the centrosome axis, while some cells also exhibited multiple IcL-DZs (n=30/65 cells) (Figure 1–figure supplement 2, Figure 1–figure supplement 3B; Video 1). Rotation along other axes did not reveal any hidden IcL-DZs (Figure 1–figure supplement 2). Our constructed DNA satellite heatmap of both the α-satellite and cenpb sequences showed a valley/depression coincident with the centrosome axis, representing IcL-DZs for multiple cells in this region (Figure 1F). These results support an IcL-DZ pattern of DNA satellites that is conserved among HUVECs along the centrosome axis.

In addition to DNA satellite sequences, the CENP-B protein has also been implicated as an interchromosomal linkage component (Kuznetsova et al., 2007). To test whether the CENP-B protein showed a similar localization pattern as the satellite sequences, we next performed IF for CENP-B, and γ-tubulin in HUVECs (Figure 1G-I). Like our DNA satellites survey, CENP-B positive centromeric associations were more visible at metaphase as compared to other stages (Figure 1H). Similarly, an IcL-DZ with an average width of 0.81 μm +/- 0.32 μm s.d. persisted across the metaphase DNA mass in individual cells (Figure 1J, n=45/58). The CENP-B heatmap also exhibited a valley/depression coincident with the centrosome axis (Figure 1K). These data support a conserved IcL-DZ pattern for a protein component of interchromosomal linkages, CENP-B, along the centrosome axis in HUVECs.

To test whether there is a non-random position of the IcL-DZs across multiple cells, we constructed a combined inverse heatmap of our DNA satellites and CENP-B protein staining. The minimal distance between positive stained centromere foci along the IcL-DZs was 0.5 μm. A 3D plate of 0.5 μm in width was used to represent each IcL-DZ (Figure 1–figure supplement 3D). The inverse heatmap revealed a high probability of IcL-DZs along the centrosome axis (Figure 1L). Hua and Mikawa (2018) demonstrated that the centrosome axis defines the

boundary of separation between haploid chromosome sets in metaphase/early anaphase cells. Therefore, we hypothesized that the DNA volumes across the IcL-DZs must be approximately equal. We then conducted a DAPI volume analysis of chromosome masses that were separated by the IcL-DZs (Figure 1M). DNA volume analysis revealed a non-random average distribution of 37% and 63% on either side of the IcL-DZ across multiple HUVECs (n=66; chi-squared: p=<0.001; Figure 1N). This set of data is suggestive, but inconclusive, whether the IcL-DZ of DNA satellite and CENP-B linkage components is the boundary between the two haploid chromosome sets (Figure 1O).

Presence of an IcL-DZ between chromosome sets in living cells at metaphase

To expand our characterization of the IcL-DZ for another cell type, and rule out the possibility of fixation effects, we tested whether the IcL-DZ could be identified in a live human retinal epithelial cell. We employed a 4D high resolution confocal imaging system, and the human CENP-A/centrin1-GFP RPE1 (RPE1) cell line, which labels the individual centromeres, and centrosomes, respectively (Magidson et al., 2011). Live cell analysis of fluorescently tagged RPE1 metaphase cells revealed an IcL-DZ, with an average width of 1.23 µm +/- 0.70 µm, along the centrosome axis (Figure 2A). The CENP-A heatmap showed a depression along the centrosome axis similar to heatmaps generated for DNA satellite/CENP-B by fixed cell analysis (Figure 2B, n=20). The inverse heatmap also showed a high frequency of centrosome based positioning of the IcL-DZs for multiple live imaged cells (Figure 2C, n=17/20). These data confirm the IcL-DZ is present in living human cells, and is not generated by fixation effects. In addition, the IcL-DZ was conserved for another human cell type, suggesting a cell type independent conserved mechanism.

Live cell tracking analysis of individual centromeres showed little mixing along the centrosome axis during metaphase (Hua and Mikawa, 2018). Volume analysis along the IcL-DZ for metaphase HUVECs suggest it may represent the boundary between the two haploid sets. To test whether the IcL-DZ persists along the centrosome axis during metaphase, when the two chromosome sets remain continuously segregated, we live imaged RPE1 cells at 30 second intervals for 5 minutes (n=5). An IcL-DZ along the centrosome axis was detected, and consistently tracked for consecutive time frames at metaphase (Figure 2D-J; Video 2). The appearance and disappearance of the IcL-DZ was dynamic during metaphase. For example, an IcL-DZ was present at multiple consecutive time points (Figure 2E-G), disappeared for 2 frames (Figure 2H, I), then became detectable at a later time point (Figure 2J). These data explain the cells without IcL-DZs in our fixed cell analysis, as they may have been fixed at a time point in metaphase when the IcL-DZ could not be identified. Our fixed cell analysis also revealed cells with multiple IcL-DZs (Figure 1–figure supplement 3B), consistent with our live cell imaging where multiple IcL-DZs could be identified within the same frame (Figure 2D, I).

An IcL-DZ along the centrosome axis was found to persist during metaphase for multiple RPE1 cells (Figure 2K, 15/17 cells). The width of the IcL-DZ fluctuated across time frames ranging from 0.55 µM to 5.24 µM, with an average of 1.44 µM+/- 0.89 µm. The data show that the IcL-DZ between chromosome sets persists during metaphase, and suggest it may be the

boundary between two haploid sets. Taken together, the IcL-DZ can be visualized in both live and fixed cells, and is conserved in a primary and established human epithelial cell line.

Ipsilateral, and apical/basal axis-based restriction of individual centromere movements along the centrosome axis from metaphase to anaphase

The persistence and position of the IcL-DZs along the centrosome axis in live cells led us to examine whether centromere fluctuations are limited by the IcL-DZ. While the IcL-DZ demonstrated dynamics of appearance and disappearance through metaphase, we found continued restriction of centromere movement parallel to the IcL-DZ in the x-, but not y-axis. The ipsilateral-based restriction of centromere movement along the centrosome axis is consistent with the orientation, or spatial distribution, of the IcL-DZ.

The IcL-DZ along the centrosome axis corresponds to a nuclear meridional, or XZ-, plane as defined by our coordinate system, and the centrin1 protein in RPE1 cells (Hua and Mikawa, 2018) (Figure 3A). The XZ-plane at metaphase defines the separation between the two haploid chromosome sets (Hua and Mikawa, 2018) (Figure 3A). Tracking of individual centromere trajectories from metaphase to anaphase were performed to determine whether individual chromosome positions were restricted relative to the IcL-DZ. Select centromeres were assigned groups (white, green), based on their initial positions along the XZ-plane at metaphase, and tracked until anaphase (Figure 3A–figure supplement 1A, A'). We found that the individual centromere trajectories show little, to no, mixing between the two groups (Figure 3B). While there were centromeres intermixing within each group, and a minor overlap between the two groups, the composite tracks of the two groups are mostly separated from metaphase to anaphase (Figure 3C), a result consistent with our previous report of continuous segregation of the two groups along the centrosome axis, or XZ-plane (Hua and Mikawa, 2018).

To test whether there is centromere mixing in other 3D planes, centromeres were grouped based on their positions on either side of the XY-plane, or the apical/basal axis, and tracked (Figure 3D–figure supplement 1B, B'). The data showed the two groups did not mix along the XY-plane, similar to the XZ-plane (Figure 3E). Examination of the individual centromere positions in the two groups showed that the centromere movements were restricted within the apical, and basal halves of the cell (Figure 3E). The composite trajectories displayed a clear separation between the two groups (Figure 3F). The YZ-plane is perpendicular to both the XZ-, and XY-planes (Figure 3G). Chromosomes continuously oscillate along the centrosome axis at metaphase alignment, before segregation to the daughter cells (Walczak et al., 2010). Unlike the clear separation in the XZ- and XY-planes, the composite trajectories of the two groups along the YZ-plane displayed a high level of overlapping, and intermingling of centromere tracks (Figure 3H, I). Therefore, the YZ-plane can serve as a negative control that shows centromere mixing from metaphase to anaphase. The data suggest that centromere movements are ipsilateral, and apical/basal restricted, specifically along the corresponding XZ- and XY-planes, but not in the YZ-plane.

To quantify the above qualitative analysis, individual centromere trajectories within the two groups at each timepoint for the three planes were analyzed (Figure 3J). For each timepoint in one cell, the average percentage of white and green centromeres that crossed the designated planes were calculated (n=20 cells) (Figure 3J–figure supplement 1C-F). The quantification analysis revealed that individual centromeres display restricted movements along the XZ-, and XY-planes, with an average of 10% centromere crossovers (Figure 3J). In contrast, the YZ-plane, with mixing of centromere groups, displayed an average of 30% centromere crossovers (Figure 3J). This result is consistent with our previous data (Hua and Mikawa, 2018), and others (Shelby et al., 1996; Skibbens et al., 1993) showing restricted centromere movements when attached to the mitotic spindle. Taken together, the data support an ipsilateral, apical/basal axis-based restriction parallel to the IcL-DZ from metaphase to anaphase. However, the mitotic spindle is intact during these stages, and may influence centromere and chromosome dynamics. We next investigate centromere positions following mitotic spindle disassembly to test whether individual chromosome fluctuations are impacted.

Individual centromere positions are maintained from telophase to G1 interphase after mitotic spindle disassembly

During metaphase/anaphase, the mitotic spindle has been reported to play a role in facilitating chromosome movements (Koshland et al., 1988; Shelby et al., 1996). Following mitotic spindle disassembly at telophase, there has been conflicting data for its impact on chromosome positions at G1 interphase (Gerlich et al., 2003; Essers et al., 2005; Walter et al., 2003; Thomson et al., 2004). To test whether the ipsilateral, apical/basal-based restriction of centromere movements is present in the absence of the mitotic spindle, we performed live cell imaging of the RPE1 cells from telophase to G1 interphase. RPE1 cells spend up to 8 hours in G1 interphase, therefore, we live imaged RPE1 cells for a minimum of 10 hours (Chao et al. 2019). To minimize phototoxicity and photobleaching, time lapse movies were captured at 30 min frame intervals to allow for longer imaging duration.

Individual centromeres of the daughter cells were grouped at telophase as previously by their positions on either side of the three planes (Figure 3A, D, and G). The centrosome axis cannot be determined after telophase due to the separation of daughter cells at cytokinesis (Cooper, 2000). At telophase, the nuclear membranes reform, and the daughter cells will flatten at G1 interphase (Lewis and Lewis, 1917). The majority of the daughter cells (n=12/14) were also motile during interphase (Figure 4A-F; Video 3). Individual tracks of the two centromere groups showed the centromeres maintain their positions along the XZ-plane from telophase to G1 interphase (Figure 4A). Composite trajectories in the XZ-plane showed collective, and restricted movement of the centromere groups (Figure 4B). To test whether the restricted centromere movements are also present in the other 3D planes, centromere tracking for groupings across the XY-, and YZ-planes were completed (Figure 4C-F). Centromere positions of the two groups in the XY-, and YZ-planes also show conserved positions to each other (Figure 4C, E). Composite trajectories of centromeres in the XY-, and YZ-planes showed a similar pattern as the XZ-plane (Figure 4D, F). This data show individual centromeres move collectively together, and maintain their positions to each other from telophase to G1 interphase.

To capture centromere movements from an intact spindle at metaphase to its disassembly at telophase, we performed live cell imaging with centromere group labeling along the centrosome, or XZ-plane for 1-1.5 hours. Time lapse movies were acquired at higher temporal resolution of 30 sec time frames to capture the dynamic movements of the chromosomes from metaphase to G1 interphase (Figure 4G; Video 4). Individual centromeres were grouped by the centrosome axis, or XZ-plane, at initial time point at metaphase, and tracked (Figure 4G). Centromere groups did not mix after spindle disassembly. This result is consistent with the data from telophase/G1 acquired at 30 minute time frames (Figure 4A-F). Minimal overlap of the composite trajectories confirmed that the ipsilateral, apical/basal axis-based restriction of centromere movements are preserved from metaphase to early G1 (Figure 4H). This data suggest that centromere positions of the two haploid sets are conserved from metaphase to completion of G1 interphase. There is little, or no, centromere reorganization even after detachment from the mitotic spindle in the RPE1 cells. Taken together, the data suggest that the IcL-DZ boundary between haploid sets, present at metaphase, remains after spindle disassembly in G1 interphase.

Ipsilateral-based restricted centromere movements at prophase prior to mitotic spindle assembly

The ipsilateral, apical/basal axis-based restriction of centromere movements from metaphase to G1 interphase prompted us to question whether these behaviors would also be seen at mitosis onset, before spindle assembly (Walczak et al., 2010). To examine whether individual centromere positions are restricted prior to spindle formation, we conducted a retrograde live cell imaging analysis from prophase to metaphase (Figure 5A; Video 5). At prophase, chromosomes undergo condensation, and become structurally visible in the cell (Gorbsky, 1992). Prior to metaphase, it is difficult to establish a reproducible axial coordinate system as centrosome positions undergo dramatic positional changes (Hua and Mikawa, 2018; Magidson et al., 2011). The centromere groupings were established at metaphase by identifying the centrosome axis, or XZ-plane (Figure 5A). Centrosomes were identified at metaphase by their positions outside of the chromosome mass, and tracked in reverse, or retrograde, to their positions at prophase (Kaseda et al., 2011) (Figure 5A–figure supplement 1). The individual centromeres were tracked forward from prophase to metaphase, with their groupings established at metaphase (Figure 5B). Examination of the centromere positions at each time point revealed that the centromere groups did not mix, and the composite trajectories showed that the two groups remain segregated from prophase to metaphase (Figure 5B, C). This data show that chromosomes condense locally at prophase, and align themselves at metaphase without a major shift in positions to other chromosomes.

To test whether the individual centromere restrictions are biased in the XZ-plane, we performed a retrograde analysis for the XY-, and YZ-planes (Figure 5D-G). Individual centromeres showed little, to no, mixing in the XY-plane, suggesting that the restricted movements at metaphase were present at mitosis onset (Figure 5D, E). Individual centromeres were found to mix in the YZ-plane (Figure 5F, G). Retrograde analysis in the YZ-plane served as a negative control for

axis-based centromere movements observed in the XZ- and XY-planes. Dynamic chromosome movements at prometaphase, such as chromosome poleward oscillations, suggest mixing between the centromere groups along the YZ-plane (Walczak et al., 2010). We quantified the individual centromere trajectories, and average percentage of centromere crossovers for the three planes (Figure 5H). An average of <10%, and 20% of centromere crossovers in the XZ-, and XY-planes, respectively, confirmed the centromere groups are segregated along the centrosome, and apical/basal axes (Figure 5H). Centromere movement patterns from prophase to metaphase are similar to those observed at metaphase/anaphase (Figure 5I). Taken together, these results show that individual centromere movements are ipsilateral, restricted along the XZ-, and XY-planes, prior to mitotic spindle assembly, and remain restricted after its disassembly. The data support that the IcL-DZ boundary for an ipsilateral axis-based centromere restriction of haploid sets persists from mitosis onset to G1 interphase, even without a major contribution of the mitotic spindle.

Discussion:

This work reveals a previously unrecognized ipsilateral, apical/basal axis-based restriction of centromere movements from mitosis onset to G1 interphase in human cells. The ipsilateral, apical/basal axis-based restriction can be observed in conjunction with an IcL-DZ, devoid of interchromosomal linkage components. Our data demonstrate, for the first time, an IcL-DZ of satellite DNA, CENP-A, and CENP-B protein linkage components along the centrosome axis (Figure 1, Figure 2). The IcL-DZ, along the centrosome axis, is the boundary between two chromosome sets, and was clearly identified in both fixed and live human epithelial cells. We have previously defined a haploid chromosome set organization across the centrosome axis in multiple cell types (Hua and Mikawa, 2018). 4D quantitative data of the spatial distribution of interchromosomal linkage components, and persistence of the IcL-DZ along the centrosome axis during metaphase supports the IcL-DZ as the boundary between two haploid chromosome sets (Hua and Mikawa 2018). Taken together, the axis-based restriction of centromere movements from mitosis onset to G1 interphase, and presence of an IcL-DZ boundary, suggests the persistence of haploid sets throughout the cell cycle in human cells (Figure 6).

Surprisingly, the IcL-DZ patterns as a plate-like gap between the chromosome sets. It is unclear how this plate-like gap structure functions or is established as a boundary between chromosome sets. Interchromosomal linkages between the chromosomes of a haploid set alone would not explain the rigidity of a plate-like IcL-DZ that may regulate haploid set organization. Pronuclear envelope proteins have been shown to contribute to parental genome separation in human and bovine embryos by forming a physical partition between parental genomes (Cavazza et al., 2021). A similar molecular/cytoskeletal plate could be acting to partition the haploid sets from each other in human cells. The plate-like IcL-DZ along the centrosome axis could then be a result of the bilateral segregation of the chromosome sets. However, there have been little to no studies describing such a molecular partition in human cells; therefore, closer investigation is needed.

Other mechanisms may be involved to regulate haploid set organization. As mentioned, a molecular or cytoskeletal barrier or cage could work together with the IcL-DZ to partition or encapsulate the chromosomes within each haploid set. Parental origin or epigenetic identity may also be implicated in haploid set organization (Hua et al., 2022). Previously, we have shown that a maternally derived translocation chromosome segregates within the same nuclear hemisphere as the X chromosome in male mouse fibroblasts (Hua and Mikawa, 2018). This suggests that the individual haploid sets may be defined by parental origin. Past studies also show DNA connectives between individual chromosomes in prematurely condensed mouse oocytes (Dozortsev et al., 2000). Thus, DNA interchromosomal linkages may be established during meiosis, and work together with the IcL-DZ to keep the maternal, and paternal genomes spatially separated after fertilization. Separation of mammalian parental genomes at fertilization and early embryonic stages has previously been reported (Reichmann et al., 2018; Destouni et al., 2016). Therefore, the linkages present could be the remnants, or consequences of this spatial segregation of parental genomes. As such, a parental haploid set identity may be inherited, and transmitted throughout the development of the organism.

Individual chromosomes from metaphase to anaphase display ipsilateral, apical-basal axis-based restriction of movements along the centrosome axis (Figure 3). A result consistent with our previous study (Hua and Mikawa, 2018) and others (Magidson et al., 2011; Brunet and Vernos, 2001), however, our previous interpretation that the restricted centromere movements along the centrosome axis as a consequence of the haploid set organization needs to be revised. The current data suggest that the restricted centromere movements are likely a combination of mitotic spindle influence, and the presence of the IcL-DZ that contribute to a continued segregation of two chromosome sets during metaphase/anaphase.

Currently, there is a lack of consensus regarding chromosome behavior throughout the cell cycle. Our data demonstrate that individual centromeres do not mix, but move collectively, and maintain their positions to each other from mitosis onset to G1 interphase (Figure 4). This result is consistent with previous studies that utilize photobleaching experiments labeling regions of the interphase nucleus to show the chromosomes did not reorganize their positions throughout the cell cycle (Gerlich et al., 2003; Essers et al., 2005). However, other groups found that chromosome positions changed during the cell cycle by motion analysis of specific loci that showed increased chromatin mobility from mitosis to G1 interphase (Walter et al., 2003; Thomson et al., 2004). One possibility for these conflicting studies could be experimental methodology, cell type differences, and data analysis/interpretation. Our analysis utilizes the CENP-A/centrin-1 GFP RPE1 cell line to track individual centromere positions, compared to tracking large subsets of chromosomes via photobleaching. Also, taken into consideration, different cell lines including HeLa cells, human fibrosarcoma cells, CHO cells, and NRK epithelial cells were used for these studies. There may be variation in chromosome movements among cell lines.

While 4D high resolution live cell imaging allows us to map individual centromere trajectories throughout the cell cycle, it would be advantageous to label the homologous chromosomes. Our analysis tracks CENP-A GFP signals for all centromeres over time, but does not provide

identification of homologous chromosomes. Live imaging systems using fluorescent transcription activator-like effector (TALES), or Clustered regularly interspaced short palindromic repeats and CRISPR-associated protein 9 (CRISPR/Cas9) have been used to visualize centromeres/telomeres consisting of repetitive genomic sequences in mouse and human cell lines (Miyanari et al., 2013; Zhou et al., 2017). Although technically challenging due to the high condensation of chromosomes, chromatin inaccessibility, and photobleaching, labeling of homologous-specific DNA loci will be necessary to definitively track chromosomes. Additionally, it would be ideal to perform live cell imaging and tracking of centromere movements for multiple cell cycles to test cell viability, but such experiments are limited by photobleaching.

Loss or gain of function (LOF)/(GOF) assays to the IcL-DZ, or interchromosomal linkages would be very difficult, if not impossible, at this time. We do not know yet how the IcL-DZ is established and maintained throughout the cell cycle, and the full interchromosomal linkage DNA identity has not been identified. Further study will be necessary to understand the relationship between interchromosomal linkages, ipsilateral chromosome movements, and bilateral segregation of haploid sets along the centrosome, and apical/basal axes. In this study, we observe the distribution of α-satellite/cenpb sequences to characterize interchromosomal linkages. Centromeric α-satellite/cenpb sequences serve as the major structural DNA component of the centromeres (Thakur et al., 2021; Rudd and Willard, 2004). As such, conducting perturbations to directly test the function of α-satellite/cenpb-based linkages for haploid set organization is not possible without impacting mitosis. To add to the complexity, linkage identity may also be different between specific chromosome groups. For example, rDNA specific linkages have been reported between the short arms of acrocentric chromosomes (Potapova et al., 2018). Sequencing data, including Hi-C data of the human genome, demonstrate that interchromosomal interactions are enriched between certain chromosome pairs (Lieberman-aiden et al., 2009). These datasets could be used for screening, and identifying additional DNA sequences within the linkages. Future studies for characterization of the interchromosomal linkages would allow for precise targeting, and enable direct LOF/GOF tests for haploid set organization.

Our findings reveal new insights into chromosome organization and dynamics. We build upon the previous model of haploid chromosome set organization along a subcellular axis to describe, for the first time, an ipsilateral, apical-basal axis-based restriction of chromosome movements along an IcL-DZ devoid of interchromosomal linkage components in human cells. Implications of our study will contribute new knowledge of genome organization and shed light onto mechanisms that are implicated in human disease.

Materials and Methods:

Cell culture:
Primary human umbilical vein endothelial cells (HUVECs, ATCC: PCS-100-013), and the human retinal pigment epithelial cell line (CENP-A/centrin1-GFP RPE1) were grown and cultured as previously described (Hua and Mikawa, 2018).

Cell selection:
Fluorescence-activated Cell Sorting (FACS) was performed for enrichment of a CENP-A/centrin1-GFP RPE1 cell population with high GFP expression. The RPE1 cell line (Magidson et al., 2011) is a heterogeneous population co-expressing CENP-A-GFP and centrin1-GFP. Cells were trypsinized, and spun down to form a cell pellet, and resuspended in 1X PBS with 5% FBS. Cell counts were then performed (1.3x10^6 cell/ml actual concentration) before transferring the cell suspension into a 5ml round-bottom FACS tube with a 35 µm cell-strainer cap (Falcon, Cat#352235). Cell suspension was kept on ice until sorting. Sony SH800 FACS (Helen Diller Building, UCSF Mission Bay Campus) was used to measure the distribution range of GFP fluorescence. Cells were bulk sorted for the top 50-85% GFP fluorescent signal, and then transferred into cell culture plates. Cells expressing the top 15% GFP fluorescence were excluded, as GFP overexpression is correlated with cellular defects, and death (Yoshihiro Mori et al., 2020). 70% of the sorted RPE1 cells are diploid based on chromosome painting (data not shown).

Immunolabeling and fluorescent in situ hybridization (ImmunoFISH):
HUVECs were grown on PTFE glass slides (Electron Microscopy Sciences, Cat# 63416-08) to 70-80% confluence for immunoFISH. Slides were washed with 1x DPBS (Gibco, Cat#14190250) twice before fixation with fresh 4% paraformaldehyde. After fixation, slides were washed 3X with chilled 1x PBS on ice, then underwent heat-induced antigen retrieval for 10 min in a sodium citrate buffer solution (10mM sodium citrate, 0.05% Tween-20, pH 6.0) in a steamer. Slides were then washed in a permeabilization buffer (0.25% Triton X-100 in 1x PBS) for 10 min followed by three 1x PBS washes at room temperature (RT). Slides were covered with a blocking buffer (10% goat serum, 0.1% Tween-20 in 1x PBS) for 30 min at RT. Slides were incubated with a primary antibody to γ-tubulin [1:1000, abcam: Anti-γ tubulin antibody (ab11317)] diluted in 0.1% Tween-20, 10% goat serum in 1x PBS. Slides were then covered in Parafilm, and incubated at 4°C in a humidified chamber overnight (O/N). The slides were washed 3x in 1x PBS. Slides were then incubated with a secondary antibody to goat anti-rabbit IgG [1:500, abcam: Goat Anti-Rabbit IgG H&L (Alexa Fluor® 647) (ab150079)] in 0.1% Tween-20, in 1% BSA and 1x PBS), covered in Parafilm, and incubated in the dark for 1 hr at RT. Slides were then washed twice with 1x PBS, and incubated with an EGS crosslinker solution (25% DMSO, 0.375% Tween-20, 25mM EGS in 1x PBS) for 10 min in the dark. Slides were washed 2x with 1x PBS, and dehydrated via chilled ethanol series on ice (70%, 80%, 100%). DNA FISH probes to α-satellite (CENT-Cy3, pnabio, F3003) and cenpb (CENPB-Alexa488, pnabio, F3004) sequences were pre-warmed at 85°C for 10 min before use. Probes were diluted in a hybridization buffer [1:50, 60% ultrapure formamide (Fisher BioReagents, Cat# BP228-100), in 20mM Tris-HCl buffer], prior to slide incubation for 5 min at 85°C. Probes diluted in hybridization buffer (5 µl) were added to slides, and incubated at 85°C for 10 min. Slides were transferred to a humidified chamber, and incubated in the dark for 2 hrs at RT. Coverslips were removed, and slides were washed in pre-warmed post-hybridization buffer (1% Tween-20, 10% 20x SSC in diH_2O at 60°C) for 3x for 10 minutes at 60°C. Slides were counterstained with DAPI before mounting with ProLong Gold antifade (Invitrogen, Cat#P36930), and sealed with coverslips.

Fixed cell imaging:
Mitotic cells were selected by brighter DAPI fluorescence intensity compared to surrounding interphase cells, DNA morphology, and centrosome position. Prometaphase cells were identified by the wheel-like rosette organization of the chromosomes as described (Nagele et al., 1995; Bolzer et al., 2005; Magidson et al., 2011; Itoh et al, 2018). Metaphase cells were identified by chromosome alignment at the equatorial plate, with centrosomes on either side. Fixed mitotic HUVECs were imaged with a confocal microscope (Leica TCS SPE, DM2500) using a 63x/1.3NA oil immersion objective with a digital zoom of 1.5x. The image data were acquired sequentially in a four-channel mode. Z-stacks were captured using a frame size of 1,024x1,024 pixels, and processed with Leica Application Suite X software (Version: 3.5.2.18963). Confocal optical sections were reconstructed and visualized in Imaris software (Bitplane: 9.8.2). Imaris deconvolution algorithm (iterations: 10, pre-sharpening gain: 7.0) was applied, and the fluorescence level for all channels was thresholded by including 90% of each signal.

Live cell imaging:
CENP-A/centrin1-GFP RPE1 (RPE1) cells were grown on 35-mm glass bottom µ-dishes (ibidi, Cat#50-305-807). Cells were imaged in culturing medium; 37°C and 5% CO2 was maintained using a cage incubator and a stage top chamber (OkoLab). Time-lapse z-stack images were captured on an inverted Ti-E microscope (Nikon) equipped with a CSU-X1 spinning disk confocal (Yokogawa), motorized XY stage with Z piezo (ASI), 4 line laser launch (Vortan), Lambda 10-3 emission filter wheel (Sutter), quad-band dichroic ZET 405/488/561/640x (Chroma), with Plan Apo VC 100x/1.4NA and Plan Apo VC 60x/1.3NA oil objectives, and a Photometrics Prime95B sCMOS camera (Teledyne). RPE1 cells were imaged using a 488-nm laser and ET525/50m emission filter (Chroma). Z-stacks were acquired every 20-30 sec for 1 hr for mitotic cells (Figure 3, Figure 5) using the 100x/1.4NA objective, and every 15-30 min for up to 10 hours for interphase cells (Figure 4) using the 60x/1.3NA objective. Image processing was completed using Imaris software.

Identification of interchromosomal linkage diminished zones (IcL-DZ):
IcL-DZs were determined by a straight line through the cell devoid of interchromosomal linkage components in fixed cells or CENP-A-GFP foci in live cells. The IcL-DZ extended from one side of the metaphase plate along its short axis, through the DAPI+ mass, to the other side. The centrosomes were used as markers. The width of the IcL-DZ was defined by the minimal distance of staining (DNA satellite sequences, CENP-B protein, CENP-A-GFP), and found to be ~0.5 µm (Figure 1–figure supplement 3). 0.5 µm was the average diameter of a CENP-A-GFP positive centromere foci (Figure 1–figure supplement 3A, A') (Valdivia et al., 2009).

Heatmap for DNA satellite sequences, CENP-B protein, and IcL-DZs:
Fixed HUVECs at metaphase stained for DNA satellite sequences (α-satellite and cenpb) and the CENP-B protein, and live-imaged RPE1 cells at metaphase with CENP-A-GFP positive centromere foci were used to generate comprehensive heatmaps. HUVECs and RPE1 cells were 3D rotated along the centrosome axis to reveal masked IcL-DZs (Figure 1–figure supplement 2). For the inverse heatmaps, IcL-DZ bars were generated as straight 0.5 µm width bars for each IcL-DZ. Each cell could have multiple IcL-DZs. For example, for 47 metaphase

HUVECs, the average number of α-satellite/cenpb IcL-DZs per cell was ~1.74. In the fixed HUVECs, one IcL-DZ per cell was chosen for the inverse heatmap. For cells with multiple IcL-DZs, the IcL-DZ closest to the DNA center of mass was selected (Figure 1–figure supplement 3D). In the live imaged RPE1 cells, all IcL-DZs identified in the representative frame per cell were included in the inverse heatmap. 3D overlays were generated by overlaying individual cells along the centrosome, or x-axis, and the composite image was exported to ImageJ software to create a heatmap (ImageJ Interactive 3D Surface Plot plugin).

Chromosome painting:
Chromosome painting for HUVECs and CENP-A/centrin1-GFP RPE1 cells was performed as previously described (Hua and Mikawa, 2018). Whole chromosome paints for Chromosome 1 in FITC, Chromosome 4 in CFP, Chromosome 19 in Texas Red, and Chromosome X in Texas Red (Applied Spectral Imaging) were used. DNA was counterstained with SYTOX (Invitrogen, Cat# S11381), and mounted with ProLong Gold antifade (Invitrogen, Cat#P36930).

3D reconstruction and overlay of homologous chromosomes for fixed cell analysis:
Overlay generation of homologous chromosomes in multiple fixed metaphase HUVECs was performed as previously described (Hua and Mikawa, 2018).

3D distance and angular orientation measurements of homologous chromosomes:
Calculations and plot generation for 2D positional analysis, and 3D distance and angular measurements between homologous chromosomes in fixed HUVECs were performed as previously described (Hua and Mikawa, 2018).

Three-Dimensional (3D) centromere and centrosome tracking:
Individual centromeres and centrosomes were identified as CENP-A/centrin1 GFP positive signals, and were defined as 0.5 μm diameter spots (Valdivia et al., 2009). The spot object tracking algorithm (Imaris) was used to track individual centromere trajectories over time. Centromere movements were identified using the autoregression motion algorithm (Imaris). The max distance between two centromere positions (initial and final), and its actual position for two consecutive time points was determined by averaging the distance traveled by randomly selected centromeres. The max distance was 1.5 μm for RPE1 cells undergoing mitosis (Magidson et al., 2011), and 10 μm for interphase cells due to longer time frame acquisition. Manual tracking analysis of centromeres in interphase was performed due to discontinuous automatic tracking resulting from the long range centromere movements (Figure 4–figure supplement 1).

Quantification analysis of centromere crossing:
The number of centromeres that crossed over the XZ-, XY-, and YZ-planes at each time point were divided by the total numbers tracked (%) (Figure 3J, Figure 5H). For example, if 3/35 green centromeres (8.57%) and 5/40 white centromeres (12.5%) crossed over the XZ-plane, the average would be 10.54% centromere crossovers for the time point.

Acknowledgements:

We thank Dr. John Sedat for his helpful suggestions and feedback. We thank T.M. lab members (Jeanette Hyer, Rieko Asai, Zhiling Zhao) and L.L.H. laboratory members for their comments and suggestions, including Marcos Peech for assistance with CENP-B protein analysis. Live imaging data for this study were acquired at the Center for Advanced Light Microscopy- CVRI at UCSF on microscopes obtained using funding from the Research Evaluation and Allocation Committee, the Gross Fund, and the Heart Anonymous Fund. Part of this work is incorporated into a Master's thesis (C.J.C.). This work was supported in part by NSF RUI Award #2027746 (to L.L.H.), CSUPERB New Investigator Grant (to L.L.H.), SSU start up funds (to L.L.H.), NIH R01 HL148125 (to T.M.), NIH R01 HL153736 (to T.M.), and Smith Family Funds (to T.M.). P.C. and C.J.C. performed experiments; P.C., C.J.C., and L.L.H. conducted analysis; P.C., C.J.C., L.L.H., and T.M. wrote the manuscript.

Figure Legends:

Figure 1. Characterization of a diminished zone devoid of interchromosomal linkage staining of α-satellite, cenpb sequences, and the CENP-B protein in HUVECs.

(A) A human umbilical vein endothelial cell (HUVEC) at prometaphase hybridized with DNA FISH for α-satellite (red), and cenpb (green) DNA, and stained for antibodies to γ-tubulin (gray), and DNA counterstain (DAPI, blue). **(B)** As in (A), but at metaphase. **(C)** As in (A), but at anaphase. **(D, E)** As in (B), without cenpb (D) or α-satellite (E) channel. (Inset) Side view. Note: An interchromosomal linkage diminished zone (IcL-DZ) (white arrowheads) is observed along the centrosome axis. **(F)** Side view of a heatmap of combined DNA satellite staining for HUVECs at metaphase aligned along the centrosome axis (gray bars/white dots in inset) (n=33 cells). (Inset) Top view. **(G-I)** As in (A-C), but immunolabeled for CENP-B protein and γ-tubulin. **(J)** As in (H), without DNA counterstain. (Inset) Side view. **(K)** As in (F), but for CENP-B (n=58 cells). **(L)** Inverse heatmap of IcL-DZs by DNA satellite and CENP-B staining in metaphase HUVECs (n=47 cells). (DAPI staining: gray). **(M)** DNA volume measurements across the IcL-DZ for metaphase HUVECs (smaller of two volumes: yellow). (Inset) The best fit plane coincident with the IcL-DZ is used for separation. **(N)** DNA volume analysis across HUVECs with IcL-DZs (n=66 cells, chi-squared analysis: p=<0.001). **(O)** Proposed interchromosomal DNA linkage model. **(P)** Axial coordinate system in a metaphase cell. Scale bars: 2 μm.

Figure 2. Presence of an IcL-DZ between chromosome sets in living cells at metaphase.

(A) Representative frame of a live cell analysis of a human CENP-A/centrin1-GFP Retinal Pigment Epithelial (RPE1) cell at metaphase. An IcL-DZ (green arrowheads) is observed along the centrosome axis (Centrosomes are labeled as red spots). (Inset) Side view. **(B)** As in [Figure 1F], but of CENP-A signals for live RPE1 cells at metaphase (n=20 cells). (Inset) Top view. **(C)** As in [Figure 1L], but generated by CENP-A signals in live imaged metaphase RPE1 cells (n=17 cells) **(D-J)** Selected sequential time frames of a RPE1 cell live imaged during metaphase for 5 minutes. The IcL-DZ along the centrosome axis (green arrowheads) and other positions (white arrowheads) were tracked for consecutive 30 sec time frames. (Inset) A green bar was placed at

the IcL-DZ corresponding to the arrowhead. **(K)** Plot of IcL-DZ width measurements across consecutive time frames of RPE1 cells during metaphase (n=17 cells). Scale bars: 2 μm.

Figure 3. Ipsilateral, and apical/basal axis-based restriction of individual centromere movements along the centrosome axis from metaphase to anaphase.

(A) Schematic of a human CENP-A/centrin1-GFP Retinal Pigment Epithelial (RPE1) cell at metaphase. The XZ-plane (dashed red line) is defined as the plane connecting the centrosomes (red) and is perpendicular to the dish. Individual centromeres are assigned into two groups (white/green) based on their positions on either side of the XZ-plane. **(B)** Select frames of a time-lapse movie of a human RPE1 cell from metaphase to anaphase showing the positions of the individual centromeres (white/green spots) to the XZ-plane (red line). Note: Spots with lines show the position of centromeres at the previous time point. **(C)** Composite trajectories of the two centromere groups (white/green spots) labeled at metaphase, and tracked (white/green lines) to anaphase in a human RPE1 cell. Centrosomes are labeled as red spots. **(D-F)** As in (A-C) but a side view showing the XY-plane (dashed blue line), which is defined as the plane parallel to the bottom of the dish. **(G-I)** As in (A-C), but of the YZ-plane, which is defined as the plane perpendicular to the XZ-plane, and the bottom of the dish. **(J)** Quantitative plot of individual centromeres (%) that cross over the XZ-plane (red), XY-plane (blue), and YZ-plane (green) from metaphase to anaphase (n=20 cells). Scale bars: 3 μm.

Figure 4. Individual centromere positions are maintained from telophase to G1 interphase after mitotic spindle disassembly.

(A) Select frames of a time-lapse movie of a human RPE1 cell from late telophase to G1 interphase showing the positions of the centromeres (white/green spots) to the XZ-plane [as in Figure 3A]. **(B)** Composite trajectories traveled by the two centromere groups (white/green spots) labeled at telophase, and tracked (white/green lines) to G1 interphase in a human RPE1 cell. Centrosomes are labeled as red spots. **(C, D)** As in (A, B) but a side view of the XY-plane [as in Figure 3D]. **(E, F)** As in (A, B) but of the YZ-plane [as in Figure 3G]. **(G)** An initial and final frame of a time-lapse movie of a human RPE1 cell from metaphase, to early G1 with the positions of the centromeres (white/green spots) labeled to the XZ-plane. **(H)** Composite trajectories traveled by the individual centromeres in (G) from metaphase to early G1. Scale bars: 5 μm.

Figure 5. Ipsilateral-based restricted centromere movements at prophase prior to mitotic spindle assembly.

(A) Schematic of retrograde tracking approach. Centrosomes (red) were identified at metaphase based on their positions outside of the chromosome mass, and tracked in reverse from metaphase to prophase. Individual centromeres were assigned into two groups (white/green spots) at metaphase, and tracked backwards. **(B)** Select frames of a time-lapse movie of a human RPE1 cell from prophase to metaphase showing the positions of the centromeres (white/green spots) to the XZ-plane (red line). **(C)** Composite trajectories of the two centromere

groups (white/green spots) labeled at metaphase, and tracked (white/green lines) to prophase in a human RPE1 cell. (Centrosomes: red spots) **(D, E)** As in (B, C) but a side view of the XY-plane. **(F, G)** As in (B, C) but of the YZ-plane. **(H)** Quantitative plot of centromeres (%) that crossed over the XZ-plane (red), XY-plane (blue), and YZ-plane (green) from prophase to metaphase (n=8 cells). **(I)** Restricted centromere movements along the XY-, and YZ-planes from prophase to metaphase. Scale bars: 3 μm.

Figure 6. Haploid chromosome set organization may be present throughout the cell cycle.

Schematic of the IcL-DZ as the boundary between the two haploid sets present throughout the cell cycle. Ipsilateral, apical-basal axis-based centromere movements along the centrosome axis are present from prophase to G1 interphase. These data support a model that the haploid set organization is present throughout mitosis onset to interphase.

Figure 1–figure supplement 1. Planar divisions of a metaphase cell and antipairing of homologous chromosomes in HUVECs

(A) Schematic of the axial coordinate system in a metaphase cell. The XZ-plane (red outline) is defined as the plane connecting the centrosomes (gray) and is perpendicular to the culture dish. **(B)** As in (A), but showing the XY-plane (blue outline), which is defined as the plane parallel to the bottom of the dish. **(C)** As in (A), but showing the YZ-plane (green outline), which is defined as the plane perpendicular to the XZ-plane and the bottom of the culture dish. **(D)** A HUVEC at metaphase painted for chromosome 1 (green), chromosome 4 (cyan), chromosome 19 (red), and DNA counterstain (SYTOX, gray). **(E)** A metaphase HUVEC stained for antibodies to γ-tubulin (gray), and DNA counterstain (DAPI, blue). Gray dot represents the DAPI center of mass. **(E')** Zoom in view of the inset of (E). The distance between the centrosome axis (line connecting the centrosomes) and the DAPI center of mass is ~0.5 μm. Thus, 0.5 μm on either side of the DNA center of mass was determined as the "boundary zone." **(F)** Top view of a 3D overlay of chromosome 1 (green/gray) distribution of multiple HUVECs at metaphase (n=25). **(G)** Relative positions for each pair of homologous chromosome 1 (green/gray circles) when mapped to an axial coordinate system (n=25). **(H)** Distance and angular orientation of homologous chromosome 1 pairs (n=25) with an average distance of 3.1 μm and angular orientation of 10.3°. **(I)** As in (F), but for chromosome 4 (cyan/gray) (n=8). **(J)** As in (G), but for chromosome 4 pairs (blue/gray circles) (n=8). **(K)** As in (H), but for chromosome 4 pairs (n=8) with an average distance of 3.6 μm and angular orientation of 9.2°. **(L)** As in (F), but for chromosome 19 (red/gray) (n=17). **(M)** As in (G), but for chromosome 19 pairs (red/gray circles) (n=17). **(N)** As in (H), but for chromosome 19 pairs (n=17) with an average distance of 1.7 μm and angular orientation of 7.5°. Note: Cells with a chromosome whose center of mass was positioned within the boundary zone were omitted from analysis. Scale bar: 2 μm.

Figure 1–figure supplement 2. 3D rotation analysis reveals an IcL-DZ devoid of α-satellite and cenpb DNA staining in metaphase HUVECs.

(A) Similar to [Figure 1B], but completed for another metaphase HUVEC. **(B)** The HUVEC in (A) rotated 8° along the x-axis. **(C)** As in (B), but rotated 77° along the y-axis. **(D)** As in (B), but rotated 90° along the x-axis. Note: Rotation from other 3D perspectives confirms the IcL-DZ (white arrowheads) from the side view, and does not reveal any hidden IcL-DZs. **(E)** 3D rotational analysis of a metaphase HUVEC along the centrosome axis reveals an IcL-DZ. Dashed black and blue lines represent the centrosome and z-axis, respectively. Scale bars: 2 μm.

Figure 1–figure supplement 3. Generation of an inverse heatmap of IcL-DZs in metaphase HUVECs.

(A) Select frame of a timelapse RPE1 cell at metaphase. White arrowheads denote centrosomes. **(A')** Zoom in view of the box of (A). Individual centromere diameters are ~0.5 μm. **(B)** Same as [Figure 1B], but for another metaphase HUVEC. Potential IcL-DZs were identified as satellite DNA negative staining regions (α-satellite and cenpb) across the DNA mass. The minimal measurements of an IcL-DZ are greater than 0.5 μm. Note: individual cells may have multiple IcL-DZs. **(C)** As in (B), but immunolabeled for CENP-B protein and γ-tubulin. **(D)** An inverse heatmap was generated by aligning the IcL-DZs of metaphase HUVECs stained for both satellite DNA (α-satellite and cenpb, n=23 cells) and CENP-B protein (n=24 cells) along their centrosome axes and overlaid (n=47 cells). DNA surfaces were created by DAPI staining. If an individual cell contained more than one IcL-DZ, the IcL-DZ closest to the DNA center of mass was selected. Scale bars: 2 μm.

Figure 3–figure supplement 1. Centromere group selection and quantification analysis of centromere crossing.

(A) As in [Figure 3A], centromere group selection along the centrosome axis, or the XZ-plane (red line) of a metaphase RPE1 cell. The long axis of the metaphase chromosome mass was divided into five equal parts. **(A')** Centromeres at the middle region (⅕) were not used for tracking analysis as it does not allow for discrimination between two groups due to chromosome fluctuations (Centrosomes: red). **(B, B')** As in (A, A') but a side view along the XY-plane (blue line). **(C, D)** Steps for quantification analysis in [Figure 3J]. Select frames of individual centromeres of RPE1 cells within the white/green group crossing over the XZ-plane (red line). The number of spots that cross the XZ-plane at each time point were recorded and divided by the total number of spots (%). Note: the total number of spots tracked decreases overtime due to photobleaching. **(E)** Table of individual tracked centromeres that cross the plane at each time point. Individual centromeres for the white/green groups were calculated at each time point, and averaged (%). Highlighted rows represent time points in (C, D). **(F)** Plot of (E) showing the average (red line, %) for individual centromeres of both white (gray line, %), or green (green line, %) groups that cross the XZ-plane from metaphase to anaphase.

Figure 4–figure supplement 1. Manual tracking of interphase centromeres.

Select frames of a time-lapse video of a human CENP-A/centrin1-GFP RPE1 cell at G1 interphase. Manual tracking of centromeres at interphase was performed by identifying individual centromeres (4-5 spots), and tracked over time. 4 different spots are shown as examples. Scale bar: 2 μm.

Figure 5–figure supplement 1. Manual tracking analysis of centrosomes.

For [Figure 5], the centrosomes (solid arrowheads) were identified at metaphase by their location outside of the chromosome mass, then manually retrograde tracked to prophase. Scale bar: 2 μm.

Video 1. Rotation of a metaphase HUVEC along the centrosome axis.

A 3D reconstructed HUVEC at metaphase stained for α-satellite (red), cenpb (green), and γ-tubulin (gray) rotating along the centrosome axis. Line denotes IcL-DZ between positive α-satellite and cenpb staining. Scale bar: 3 μm.

Video 2. Presence of IcL-DZ between chromosome sets in a live RPE1 cell at metaphase.

A 4D time-lapse movie of a human CENP-A/centrin1-GFP RPE1 cell progressing through metaphase. Lines (green) denote IcL-DZs between CENP-A signals along the centrosome axis. Scale bar: 2 μm.

Video 3. Chromosomes move collectively from telophase to G1 interphase.

A 4D time-lapse movie of a human CENP-A/centrin1-GFP RPE1 cell from telophase to G1 interphase. Two groups of centromeres along the centrosome axis, or the XZ-plane, were labeled (white/green spots) at an initial time point at telophase, and tracked (white/green lines) until G1 interphase. (Centrosomes: red). Scale bars: 3 μm.

Video 4. Individual centromeres show minimal mixing from metaphase to early G1.

A 4D time-lapse movie of a human CENP-A/centrin1-GFP RPE1 cell from metaphase to early G1. Two groups of centromeres along the centrosome axis, or the XZ-plane, were labeled (white/green spots) at an initial time point at metaphase, and tracked (white/green lines) until early G1 interphase. (Centrosomes: red). Scale bars: 2 μm.

Video 5. Chromosomes condense locally at prophase, and maintain their positions to metaphase.

A 4D time-lapse movie of a human CENP-A/centrin1-GFP RPE1 cell undergoing mitosis from prophase to metaphase. Centrosomes (red) were identified at metaphase, and retroactively tracked to prophase. Two groups of centromeres along the centrosome axis were labeled

(white/green spots) at metaphase, and retroactively tracked (white/green lines) to prophase. Scale bars: 2 µm.

References:

1) Alcobia I, Dilao R, Parreira L (2000) **Spatial associations of centromeres in the nuclei of hematopoietic cells: Evidence for cell-type-specific organizational patterns** *Blood* :1608–1615.
2) Bloom KS (2014) **Centromeric heterochromatin: The primordial segregation machine** *Annual Review of Genetics* **48**:457–484.
3) Bolzer A, Kreth G, Solovei I, Koehler D, Saracoglu K, Fauth C, Müller S, Eils R, Cremer C, Speicher MR, Cremer T (2005) **Three-dimensional maps of all chromosomes in human male fibroblast nuclei and prometaphase rosettes** *PLoS biology* **3**:e157.
4) Boyle S, Gilchrist S, Bridger JM, Mahy NL, Ellis JA, Bickmore WA (2001) **The spatial organization of human chromosomes within the nuclei of normal and emerin-mutant cells** *Human molecular genetics* **10**:211–219.
5) Bridger JM, Boyle S, Kill IR, Bickmore WA (2000) **Re-modelling of nuclear architecture in quiescent and senescent human fibroblasts** *Current biology : CB* **10**:149–152.
6) Brunet S, Vernos I (2001) **Chromosome motors on the move** *EMBO reports* **2**:69-6673.
7) Burdick AB (1976) **Somatic cell chromosome interconnections in trypan preparations of Chinese hamster testicular cells** *Experimental Cell Research* **99**:425–428.
8) Cavazza T, Takeda Y, Politi AZ, Aushev M, Aldag P, Baker C, Choudhary M, Bucevičius J, Lukinavičius G, Elder K, Blayney M, Lucas-Hahn A, Niemann H, Herbert M, Schuh M (2021) **Parental genome unification is highly error-prone in mammalian embryos** *Cell* **184**:2860–2877.e22.
9) Chao HX, Fakhreddin RI, Shimerov HK, Kedziora KM, Kumar RJ, Perez J, Limas JC, Grant GD, Cook JG, Gupta GP, Purvis JE (2019) **Evidence that the human cell cycle is a series of uncoupled, memoryless phases** *Molecular Systems Biology* **15(3):**e8604.
10) Cooper GM (2000) **Chromosomes and Chromatin** *The Cell: A Molecular Approach. 2nd edition*. Sunderland (MA): Sinauer Associates.
11) Cremer M, von Hase J, Volm T, Brero A, Kreth G, Walter J, Fischer C, Solovei I, Cremer C, Cremer T (2001) **Non-random radial higher-order chromatin arrangements in nuclei of diploid human cells** *Chromosome research : an international journal on the molecular, supramolecular and evolutionary aspects of chromosome biology* **9**:541–567.
12) Croft JA, Bridger JM, Boyle S, Perry P, Teague P, Bickmore WA (1999) **Differences in the localization and morphology of chromosomes in the human nucleus** *The Journal of cell biology* **145**:1119–1131.
13) Destouni A, Zamani Esteki M, Catteeuw M, Tšuiko O, Dimitriadou E, Smits K, Kurg A, Salumets A, Van Soom A, Voet T, Vermeesch JR (2016) **Zygotes segregate entire**

parental genomes in distinct blastomere lineages causing cleavage-stage chimerism and mixoploidy *Genome research* **26**:567–578.
14) Dozortsev D, Coleman A, Nagy P, Diamond MP, Ermilov A, Weier U, Liyanage M, Reid T (2000) **Nucleoli in a pronuclei-stage mouse embryo are represented by major satellite DNA of interconnecting chromosomes** *Fertility and sterility* **73**:366–371.
15) Emmerich G, Scharrer Z von S, Stengel-Rutkowski S, Zang KD (1973) **Elektronenmikroskopische Untersuchung interchromosomaler fädiger Strukturen an menschlichen Lymphocyten in der Metaphase** *Human Genetics* **19**:227–234.
16) Emmerich P, Loos P, Jauch A, Hopman AH, Wiegant J, Higgins MJ, White BN, van der Ploeg M, Cremer C, Cremer T (1989) **Double in situ hybridization in combination with digital image analysis: a new approach to study interphase chromosome topography** *Experimental cell research* **181**:126–140.
17) Essers J, Cappellen WAV, Theil AF, Drunen EV, Jaspers NGJ, Hoeijmakers JHJ, Wyman C, Vermeulen W, Kanaar R (2005) **Dynamics of relative chromosome position during the cell cycle** *Molecular Biology of the Cell* **16**:769–775.
18) Gerlich D, Beaudouin J, Kalbfuss B, Daigle N, Eils R, Ellenberg J (2003) **Global chromosome positions are transmitted through mitosis in mammalian cells** *Cell* **112**:751-764.
19) Gorbsky GJ (1992) **Chromosome motion in mitosis** *BioEssays* **14**:73–80.
20) Guenatri M, Bailly D, Maison C, Almouzni G (2004) **Mouse centric and pericentric satellite repeats form distinct functional heterochromatin** *Journal of Cell Biology* **166**:493–505.
21) Hua LL, Casas CJ, Mikawa T (2022) **Mitotic Antipairing of Homologous Chromosomes** *Results and problems in cell differentiation* **70**:191–220.
22) Hua LL, Mikawa T (2018) **Mitotic antipairing of homologous and sex chromosomes via spatial restriction of two haploid sets** *Proceedings of the National Academy of Sciences of the United States of America* **115**:E12235–E12244.
23) Itoh G, Ikeda M, Iemura K, Amin MA, Kuriyama S, Tanaka M, Mizuno N, Osakada H, Haraguchi T, Tanaka K (2018) **Lateral attachment of kinetochores to microtubules is enriched in prometaphase rosette and facilitates chromosome alignment and bi-orientation establishment** *Scientific reports* **8**:3888.
24) Jaffray JY, Geneix A (1974) **Interchromosomal fibers: Human ultrastructural study by a recent technique** *Human Genetics* **25**:119–126.
25) Jagannathan M, Cummings R, Yamashita YM (2018) **A conserved function for pericentromeric satellite DNA** *ELife* **7**.
26) Jagannathan M, Yamashita YM (2017) **Function of Junk: Pericentromeric Satellite DNA in Chromosome Maintenance** *Cold Spring Harbor Symposia on Quantitative Biology* **82**:319–327.
27) Jones KW (1970) **Chromosomal and nuclear location of Mouse Satellite DNA in individual cells** *Nature* **225**:912–915.
28) Jones KW (1973) **Satellite DNA** *Journal of medical genetics* **10**:273–281.
29) Kaseda K, McAinsh AD, Cross RA (2011) **Dual pathway spindle assembly increases both the speed and the fidelity of mitosis** *Biology Open* **1**:12–18.

30) Kim SH, McQueen PG, Lichtman MK, Shevach EM, Parada LA, Misteli T (2004) **Spatial genome organization during T-cell differentiation** *Cytogenetic and Genome Research* **105**:292–301.
31) Koshland DE, Mitchison TJ, Kirschner MW (1988) **Polewards chromosome movement driven by microtubule depolymerization in vitro** *Nature* **331**:499–504.
32) Küpper K, Kölbl A, Biener D, Dittrich S, von Hase J, Thormeyer T, Fiegler H, Carter NP, Speicher MR, Cremer T, Cremer M (2007) **Radial chromatin positioning is shaped by local gene density, not by gene expression** *Chromosoma* **116**:285–306.
33) Kuznetsova IS, Enukashvily NI, Noniashvili EM, Shatrova AN, Aksenov ND, Zenin VV, Dyban AP, Podgornaya OI (2007) **Evidence for the existence of satellite DNA-containing connection between metaphase chromosomes** *Journal of cellular biochemistry* **101**:1046–1061.
34) Lesko SA, Callahan DE, LaVilla ME, Wang ZP, Ts'o PO (1995) **The experimental homologous and heterologous separation distance histograms for the centromeres of chromosomes 7, 11, and 17 in interphase human T-lymphocytes** *Experimental cell research* **219**: 499–506.
35) Lewis WH, Lewis MR (1917) **The duration of various phases of mitosis in the mesen chyme cells of tissue cultures** *The Anatomical Record* **13**:359-67.
36) Lieberman-Aiden E, van Berkum NL, Williams L, Imakaev M, Ragoczy T, Telling A, Amit I, Lajoie BR, Sabo PJ, Dorschner MO, Sandstrom R, Bernstein B, Bender MA, Groudine M, Gnirke A, Stamatoyannopoulos J, Mirny LA, Lander ES, Dekker J (2009) **Comprehensive mapping of long-range interactions reveals folding principles of the human genome** *Science (New York, N.Y.)* **326**:289–293.
37) Magidson V, O'Connell CB, Lončarek J, Paul R, Mogilner A, Khodjakov A (2011) **The spatial arrangement of chromosomes during prometaphase facilitates spindle assembly** *Cell* **146**:555–567.
38) Maniotis AJ, Bojanowski K, Ingber DE (1997) **Mechanical continuity and reversible chromosome disassembly within intact genomes removed from living cells** *Journal of Cellular Biochemistry* **65**:114–130.
39) Marella NV, Bhattacharya S, Mukherjee L, Xu J, Berezney R (2009) **Cell type specific chromosome territory organization in the interphase nucleus of normal and cancer cells** *Journal of Cellular Physiology* **221**:130–138.
40) Marko JF (2008) **Micromechanical studies of mitotic chromosomes** *Chromosome research : an international journal on the molecular, supramolecular and evolutionary aspects of chromosome biology* **16**:469–497.
41) Mayer R, Brero A, von Hase J, Schroeder T, Cremer T, Dietzel S (2005) **Common themes and cell type specific variations of higher order chromatin arrangements in the mouse** *BMC Cell Biology* **6**:44.
42) Miyanari Y, Ziegler-Birling C, Torres-Padilla M-E (2013) **Live visualization of chromatin dynamics with Fluorescent Tales** *Nature Structural & Molecular Biology* **20**:1321–1324.
43) Mora-Bermúdez F, Gerlich D, Ellenberg J (2007) **Maximal chromosome compaction occurs by axial shortening in anaphase and depends on Aurora kinase** *Nature cell biology* **9**:822–831.

44) Mori Y, Yoshida Y, Satoh A, Moriya H (2020) **Development of an experimental method of systematically estimating protein expression limits in HEK293 cells** *Scientific Reports* **10**:4798.
45) Mosgöller W, Leitch AR, Brown JK, Heslop-Harrison JS (1991) **Chromosome arrangements in human fibroblasts at mitosis** *Human genetics* **88**:27–33.
46) Muller WA, Gimbrone MA, Jr (1986) **Plasmalemmal proteins of cultured vascular endothelial cells exhibit apical-basal polarity: analysis by surface-selective iodination** *The Journal of cell biology* **103**:2389–2402.
47) Nagele R, Freeman T, McMorrow L, Lee HY (1995) **Precise spatial positioning of chromosomes during prometaphase: evidence for chromosomal order** *Science (New York, N.Y.)* **270**:1831–1835.
48) Neusser M, Schubel V, Koch A, Cremer T, Müller S (2007) **Evolutionarily conserved, cell type and species-specific higher order chromatin arrangements in interphase nuclei of primates** *Chromosoma* **116**:307–320.
49) Parada LA, McQueen PG, Misteli T (2004) **Tissue-specific spatial organization of genomes** *Genome Biology* **5**:R44.
50) Pidoux AL, Allshire RC (2005) **The role of heterochromatin in centromere function** *Philosophical transactions of the Royal Society of London. Series B, Biological sciences* **360**:569–579.
51) Potapova TA, Unruh JR, Yu Z, Rancati G, Li H, Stampfer MR, Gerton JL (2019) **Superresolution microscopy reveals linkages between ribosomal DNA on heterologous chromosomes** *Journal of Cell Biology* **218**:2492–2513.
52) Reichmann J, Nijmeijer B, Hossain MJ, Eguren M, Schneider I, Politi AZ, Roberti MJ, Hufnagel L, Hiiragi T, Ellenberg J (2018) **Dual-spindle formation in zygotes keeps parental genomes apart in early mammalian embryos** *Science (New York, N.Y.)* **361**:189–193.
53) Rudd MK, Willard HF (2004) **Analysis of the centromeric regions of the human genome assembly** *Trends in genetics : TIG* **20**:529–533.
54) Saifitdinova AF, Derjusheva SE, Malykh AG, Zhurov VG, Andreeva TF, Gaginskaya ER (2001) **Centromeric tandem repeat from the chaffinch genome: Isolation and molecular characterization** *Genome* **44**:96–103.
55) Saksouk N, Simboeck E, Déjardin J (2015) **Constitutive heterochromatin formation and transcription in mammals** *Epigenetics & chromatin* **8**:3.
56) Shelby RD, Hahn KM, Sullivan KF (1996) **Dynamic elastic behavior of alpha-satellite DNA domains visualized in situ in living human cells** *Journal of Cell Biology* **135**:545–557.
57) Skibbens RV, Skeen VP, Salmon ED (1993) **Directional instability of kinetochore motility during chromosome congression and segregation in mitotic newt lung cells: A push-pull mechanism** *Journal of Cell Biology* **122**:859–875.
58) Sun HB, Shen J, Yokota H (2000) **Size-dependent positioning of human chromosomes in interphase nuclei** *Biophysical journal* **79**:184–190.
59) Takayama S (1975) **Interchromosomal connectives in squash preparations of L cells** *Experimental Cell Research* **91**:408–412.

60) Thakur J, Packiaraj J, Henikoff S (2021) **Sequence, Chromatin and Evolution of Satellite DNA** *International journal of molecular sciences* **22**:4309.
61) Thomson I, Gilchrist S, Bickmore WA, Chubb JR (2004) **The radial positioning of chromatin is not inherited through mitosis but is established de novo in early G1** *Current Biology* **14**:166–172.
62) Valdivia M, Hamdouch K, Ortiz M, Astola A (2009) **Cenpa a genomic marker for centromere activity and human diseases** *Current Genomics* **10**:326–335.
63) Walczak CE, Cai S, Khodjakov A (2010) **Mechanisms of chromosome behaviour during mitosis** *Nature reviews. Molecular cell biology* **11**:91–102.
64) Walter J, Schermelleh L, Cremer M, Tashiro S, Cremer T (2003) **Chromosome order in Hela cells changes during mitosis and early G1, but is stably maintained during subsequent interphase stages** *Journal of Cell Biology* **160**:685–697.
65) Wijchers PJ, Geeven G, Eyres M, Bergsma AJ, Janssen M, Verstegen M, Zhu Y, Schell Y, Vermeulen C, de Wit E, de Laat W (2015) **Characterization and dynamics of pericentromere-associated domains in mice** *Genome research* **25**:958–969.
66) Zhou Y, Wang P, Tian F, Gao G, Huang L, Wei W, Xie XS (2017) **Painting a specific chromosome with CRISPR/Cas9 for live-cell imaging** *Cell Research*. **27**:298–301.

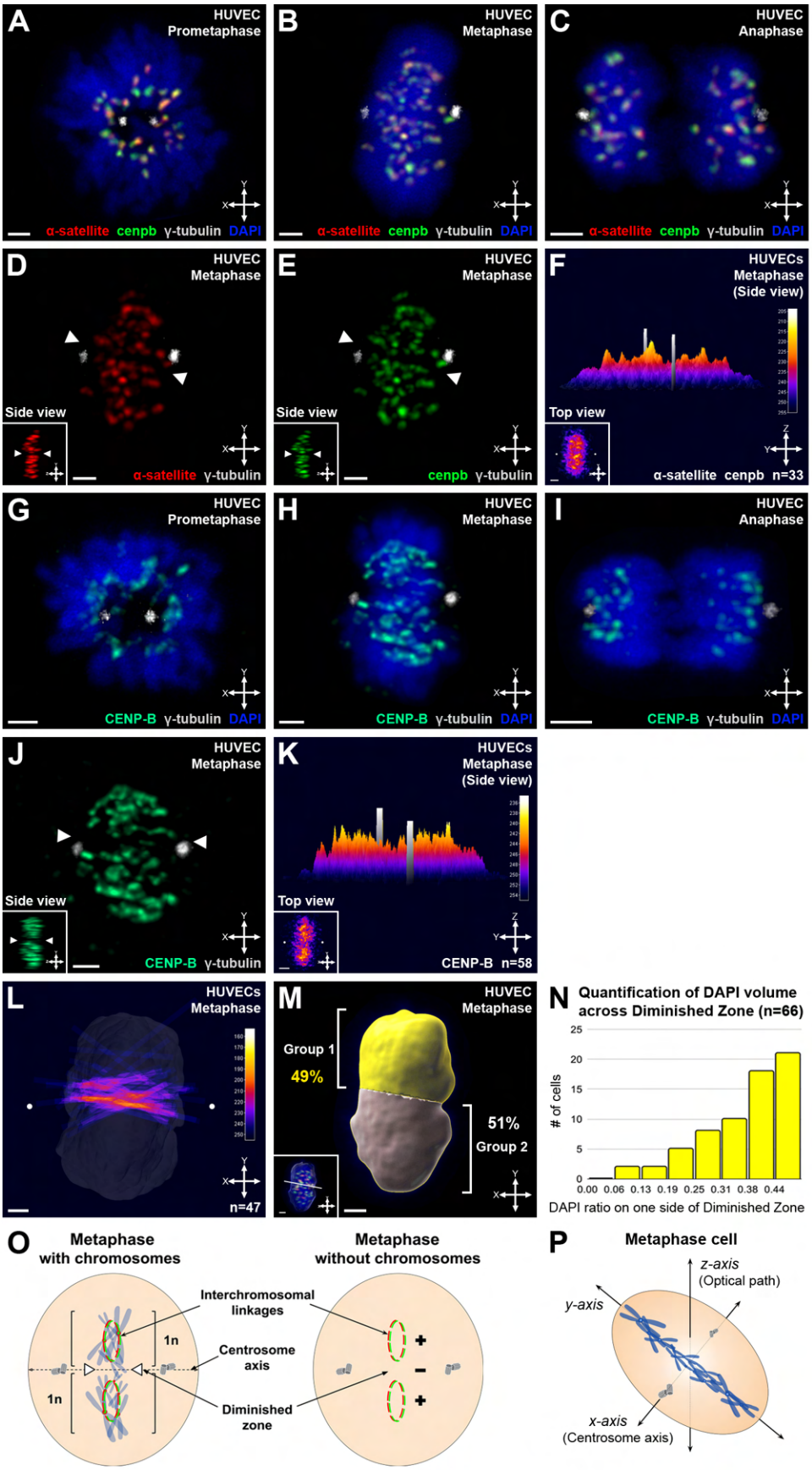

(Cai, Casas, Hua and Mikawa, Figure 1)

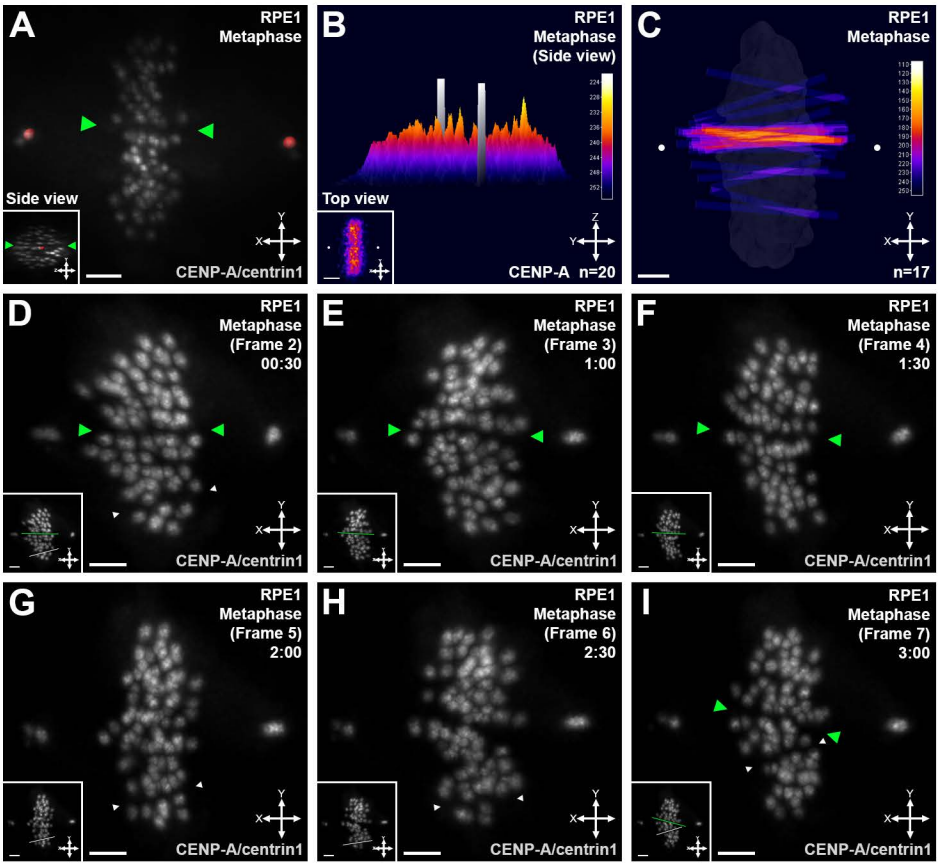

J **Quantification of presence of diminished zone during metaphase (n=17cells)**

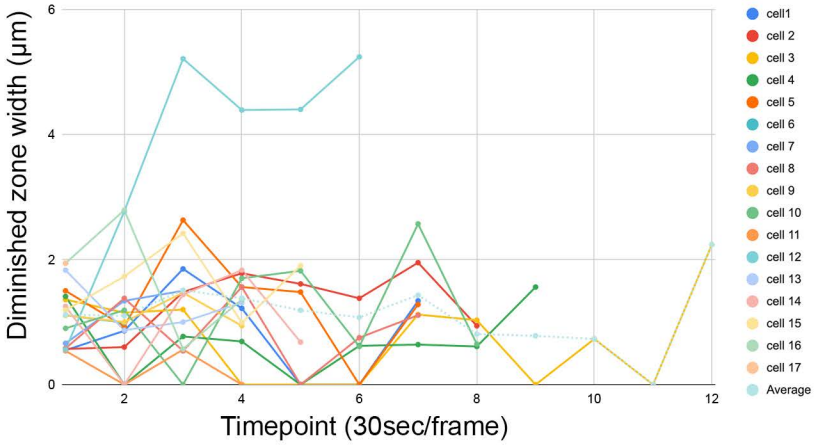

(Cai, Casas, Hua and Mikawa, Figure 2)

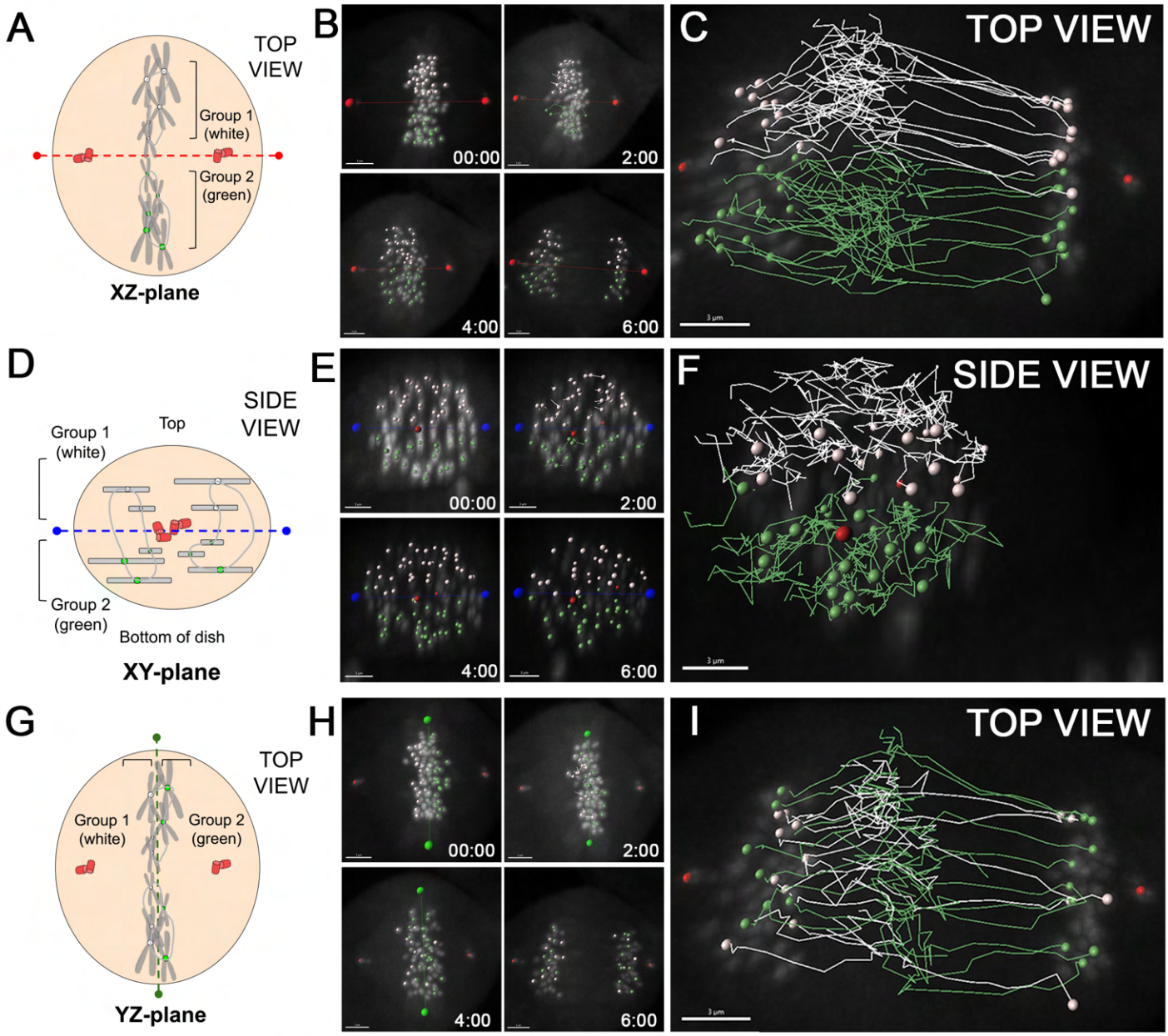

J **Quantification of individual centromeres within Group 1 or 2 crossing the designated plane (n=20 cells)**

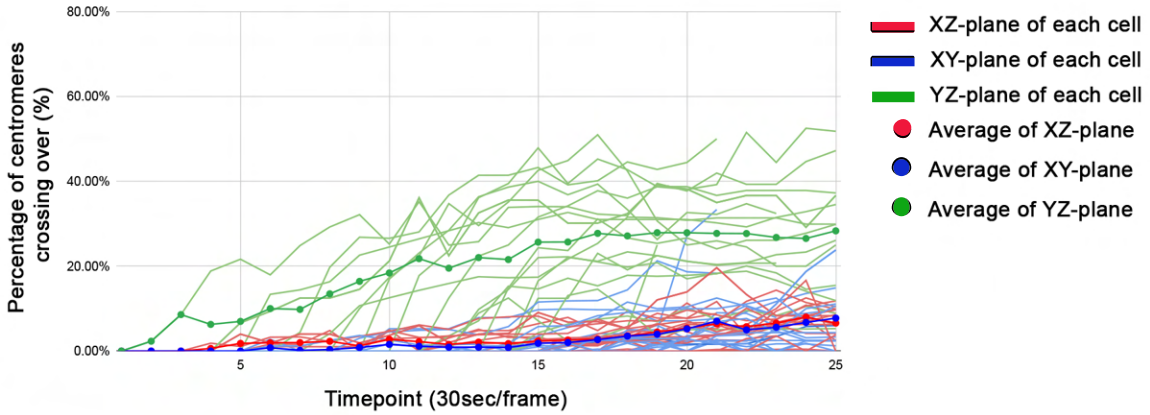

(Cai, Casas, Hua and Mikawa, Figure 3)

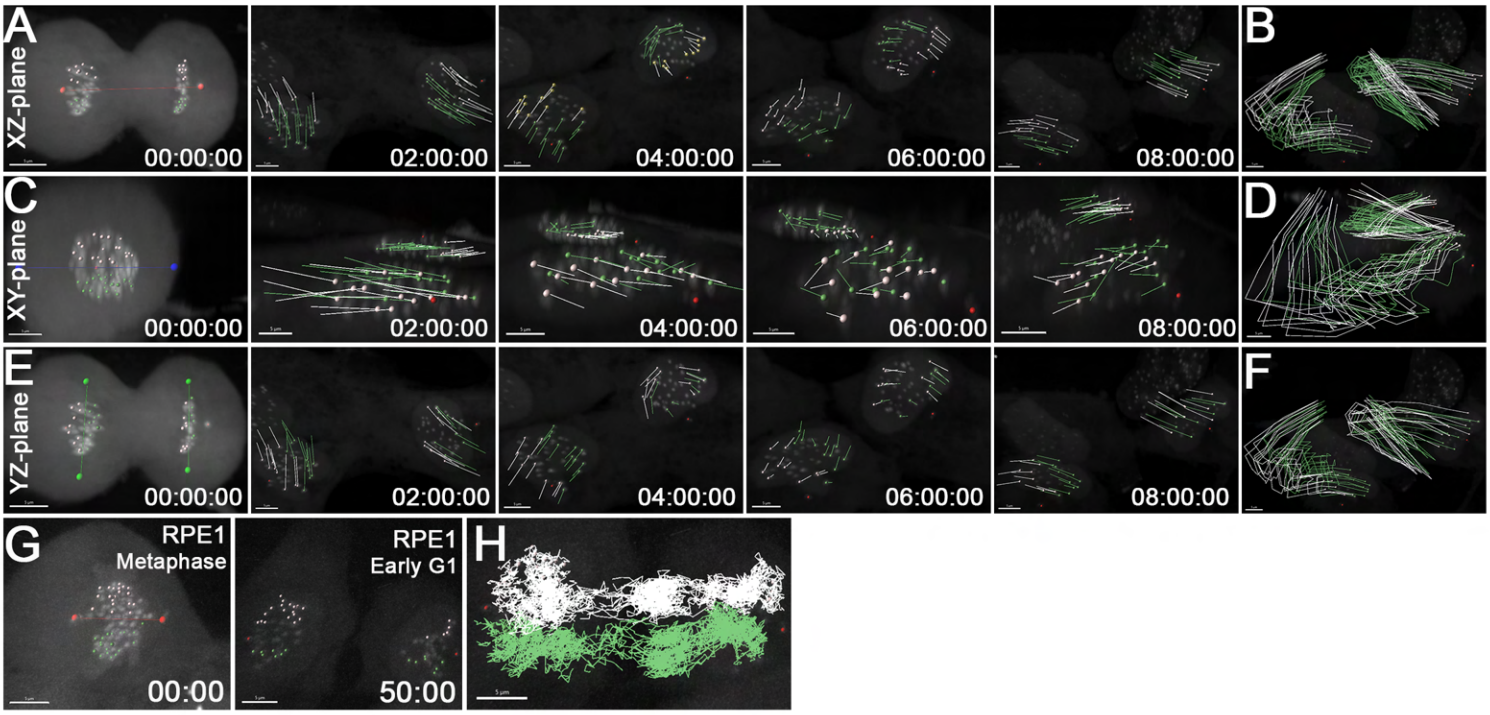

(Cai, Casas, Hua and Mikawa, Figure 4)

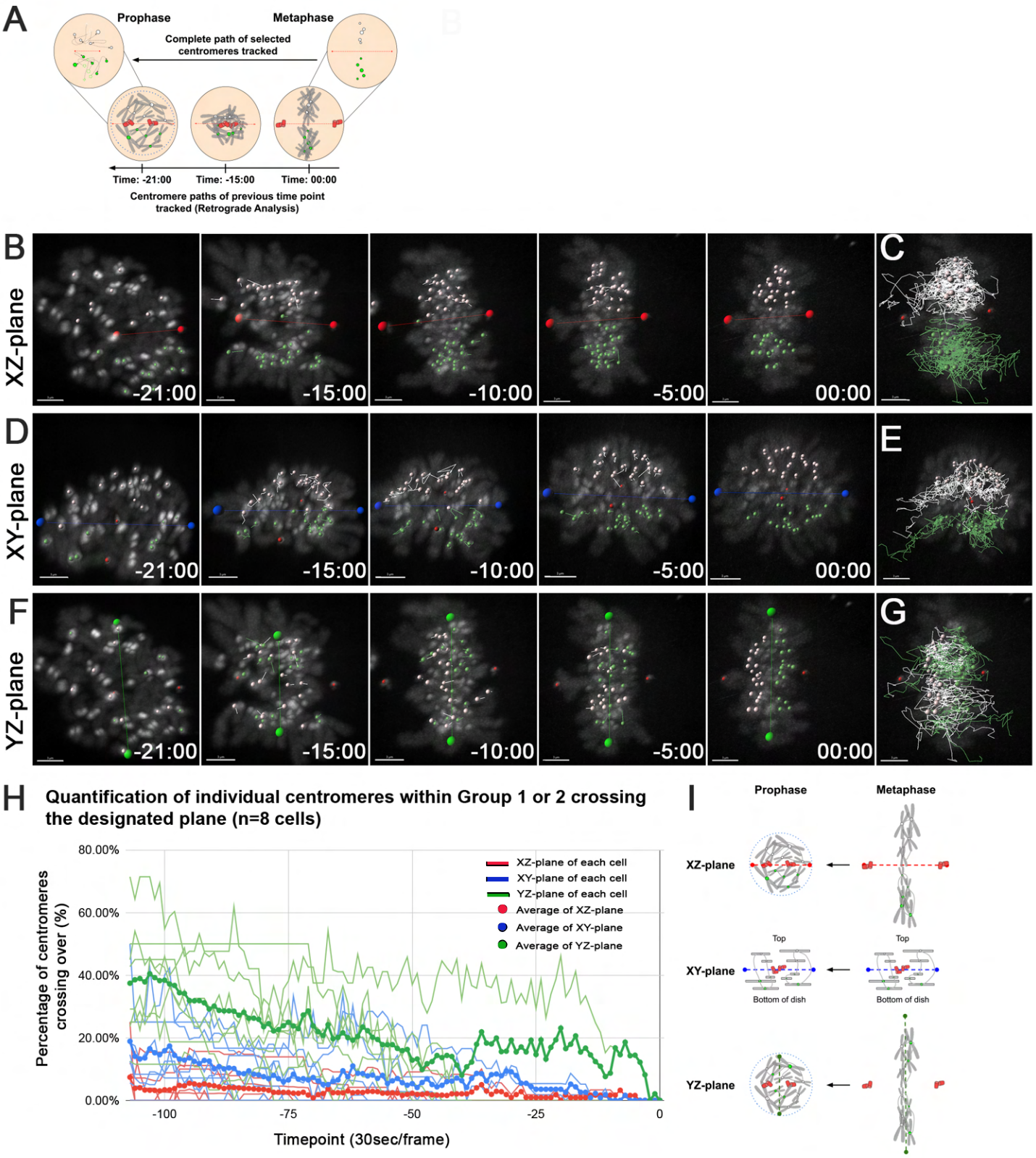

(Cai, Casas, Hua and Mikawa, Figure 5)

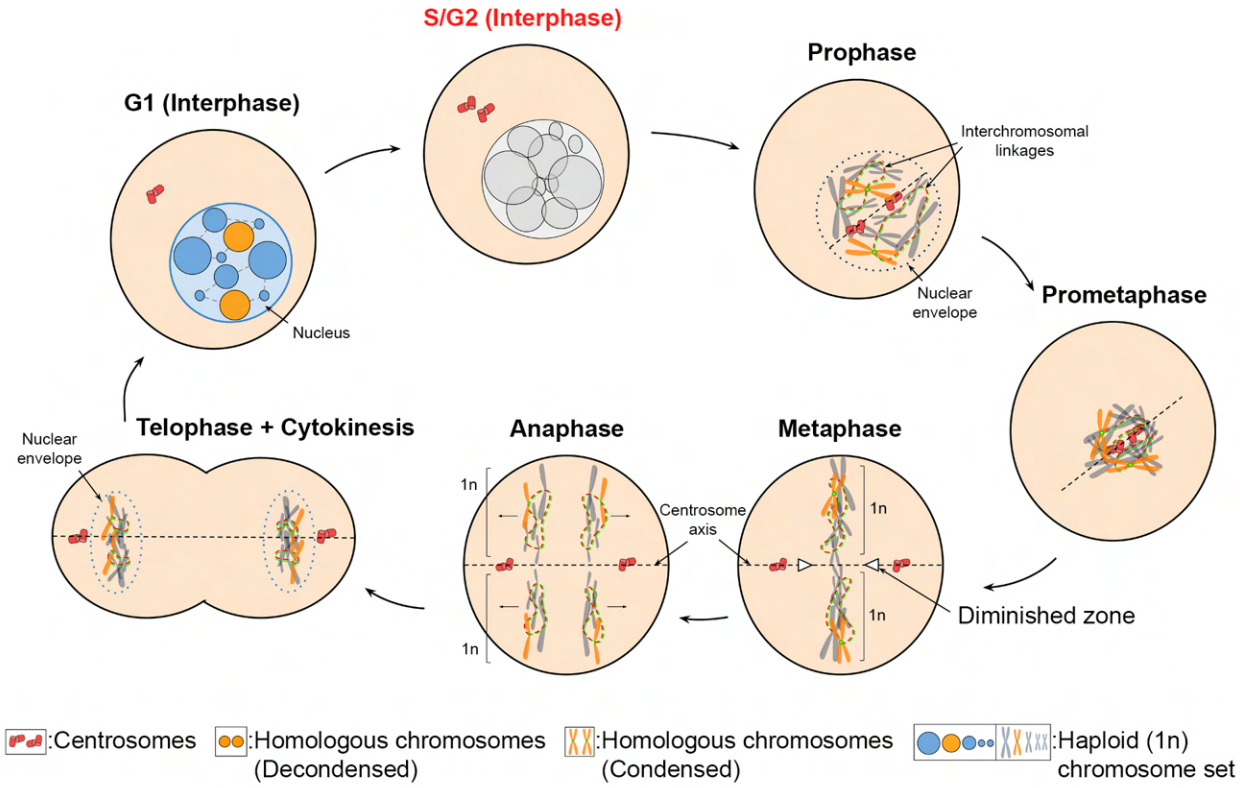

(Cai, Casas, Hua and Mikawa, Figure 6)

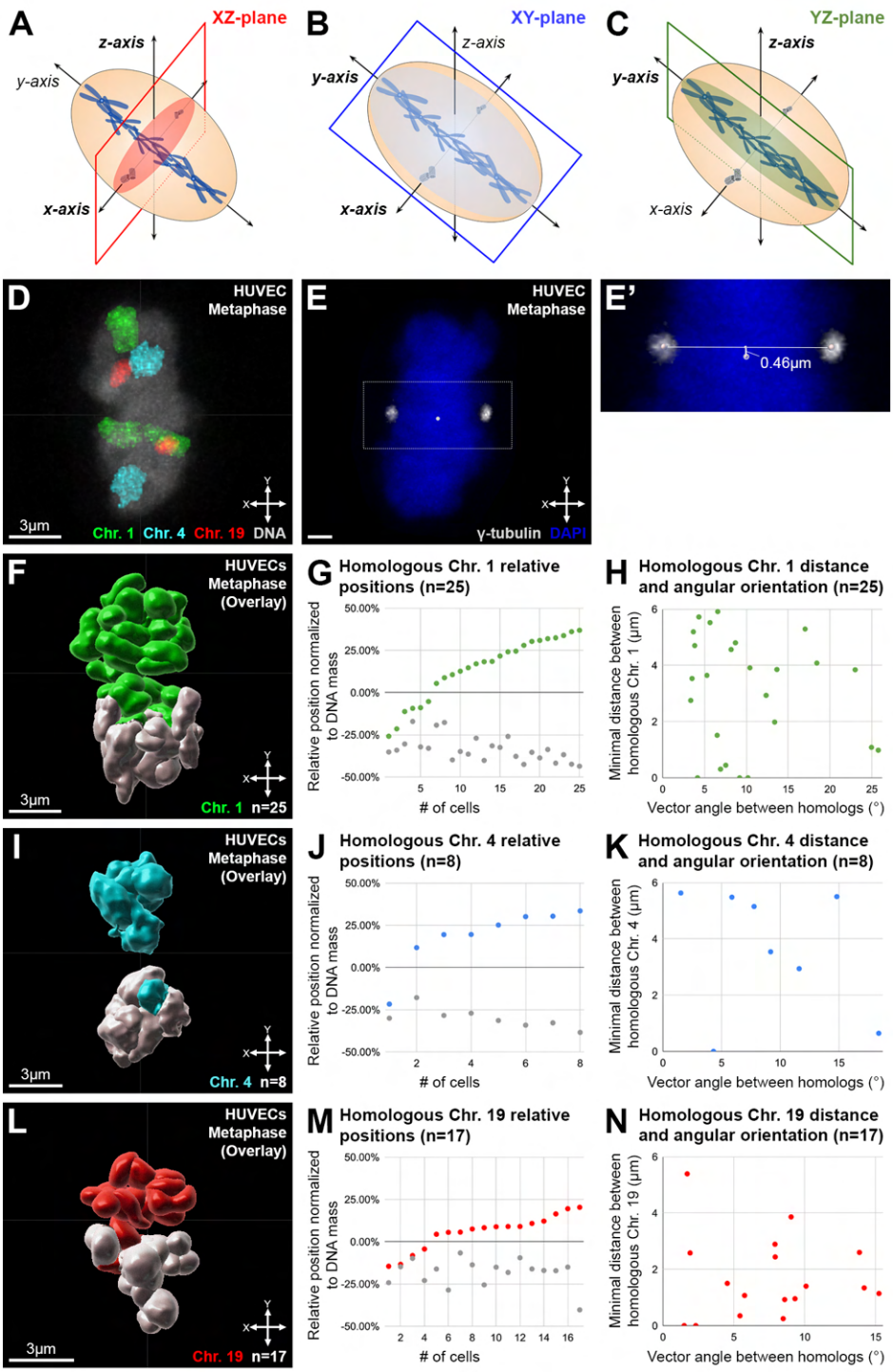

(Cai, Casas, Hua and Mikawa, Figure 1--figure supplement 1)

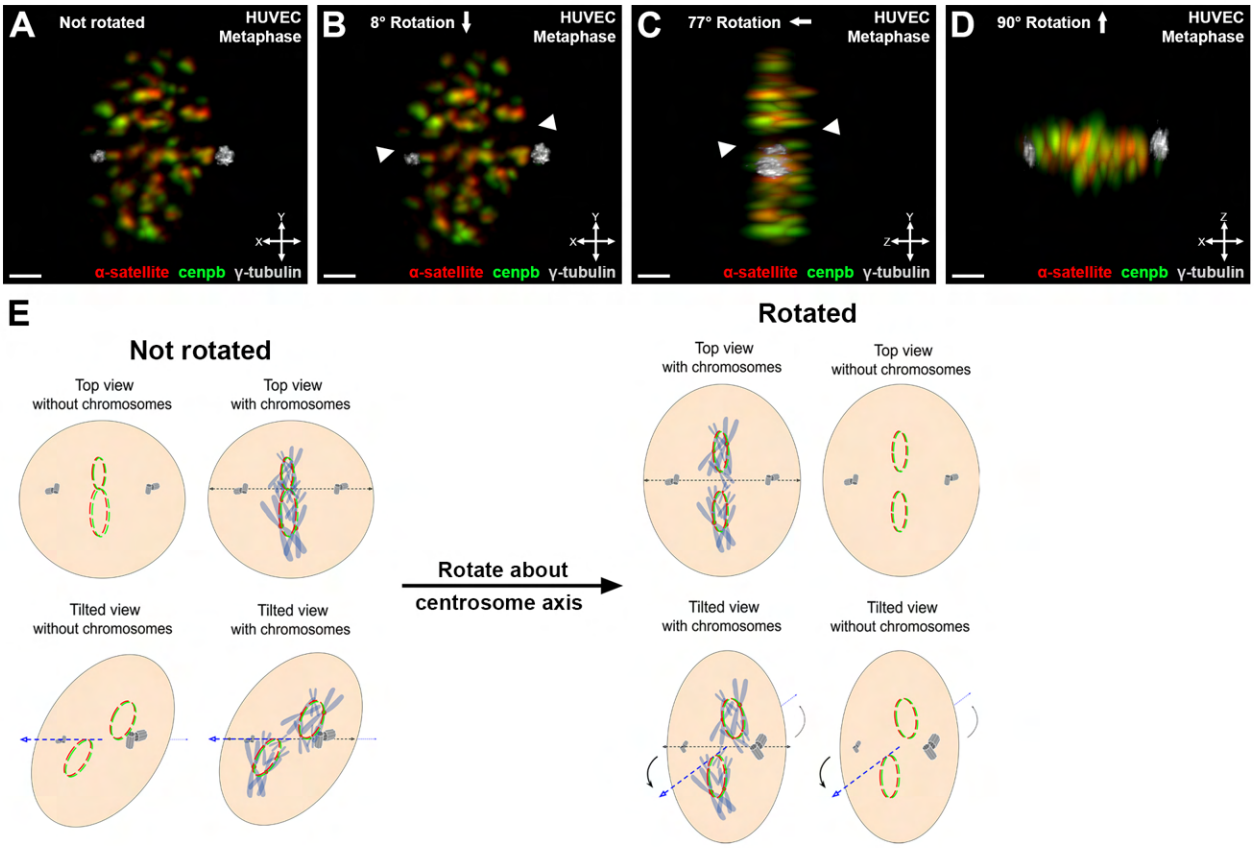

(Cai, Casas, Hua and Mikawa, Figure 1--figure supplement 2)

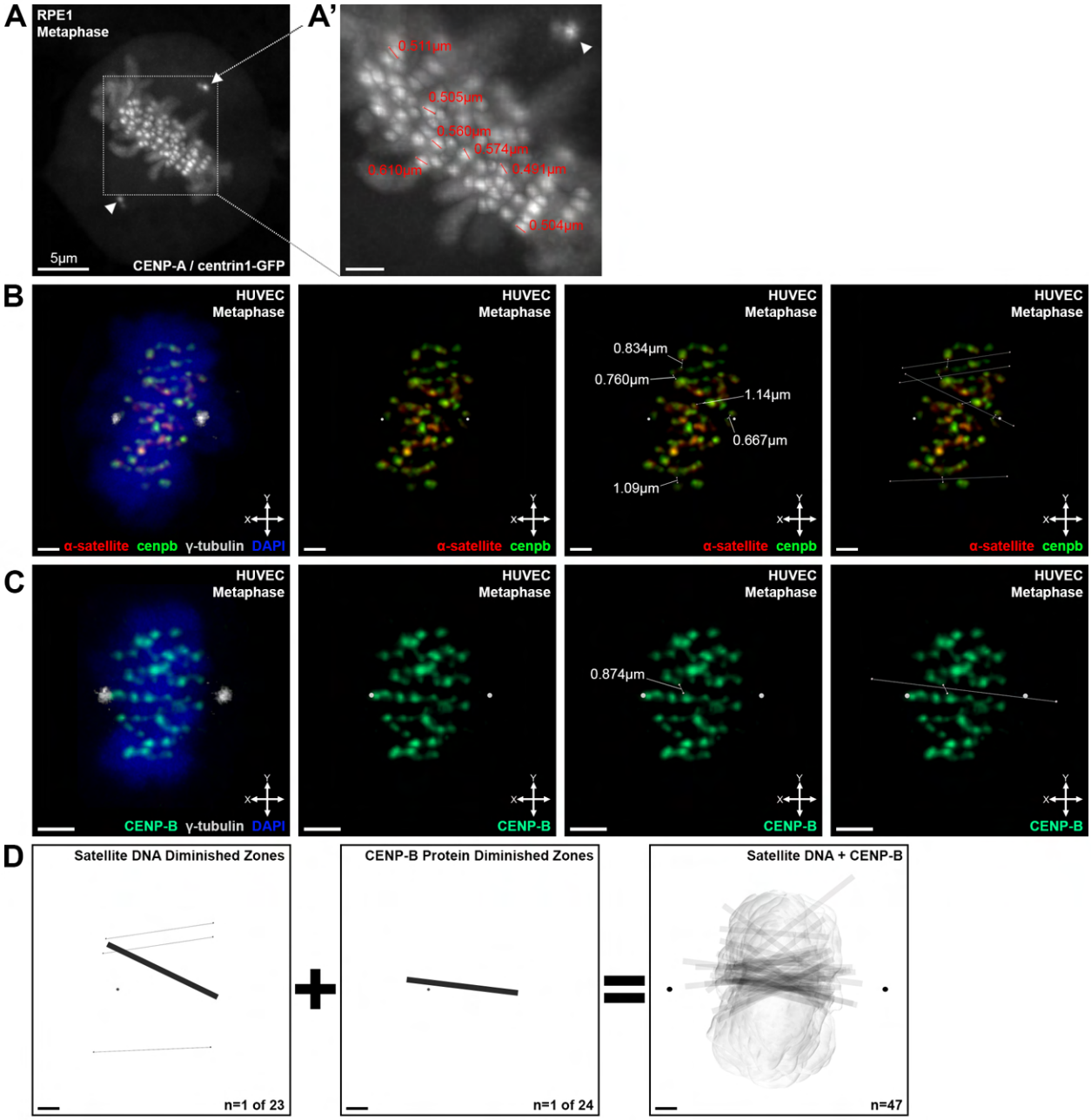

(Cai, Casas, Hua and Mikawa, Figure 1--figure supplement 3)

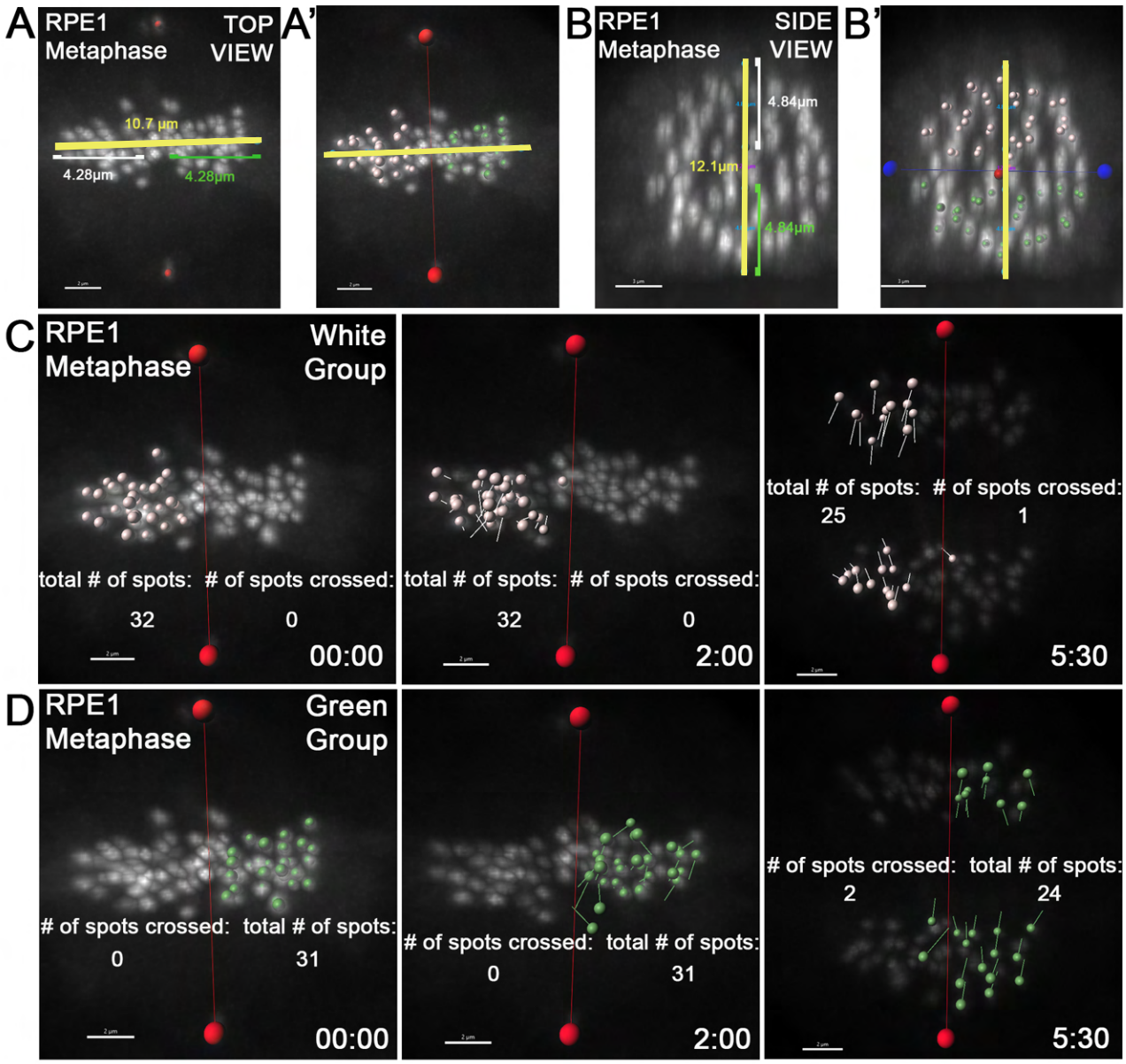

E

Timepoint	# of green spots crossed	total # of spots tracked at this timepoint	% crossed	# of white spots crossed	total # of spots tracked at this timepoint	% crossed	Average %
1	0	31	0.00%	0	32	0.00%	0.00%
2	0	31	0.00%	0	32	0.00%	0.00%
3	0	30	0.00%	0	32	0.00%	0.00%
4	0	31	0.00%	0	32	0.00%	0.00%
5	0	31	0.00%	0	32	0.00%	0.00%
6	0	31	0.00%	0	32	0.00%	0.00%
7	0	31	0.00%	0	32	0.00%	0.00%
8	0	30	0.00%	0	32	0.00%	0.00%
9	2	29	6.90%	0	31	0.00%	3.45%
10	2	28	7.14%	0	30	0.00%	3.57%
11	3	24	12.50%	0	26	0.00%	6.25%
12	2	24	8.33%	1	25	4.00%	6.17%
13	2	24	8.33%	0	25	0.00%	4.17%
14	3	24	12.50%	0	24	0.00%	6.25%
15	2	24	8.33%	0	24	0.00%	4.17%
16	2	24	8.33%	0	22	0.00%	4.17%
17	2	22	9.09%	0	19	0.00%	4.55%
18	2	20	10.00%	0	19	0.00%	5.00%

F

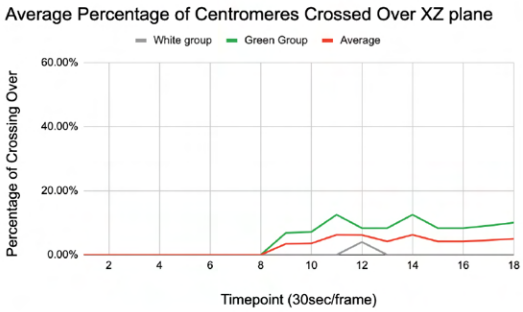

(Cai, Casas, Hua and Mikawa, Figure 3--figure supplement 1)

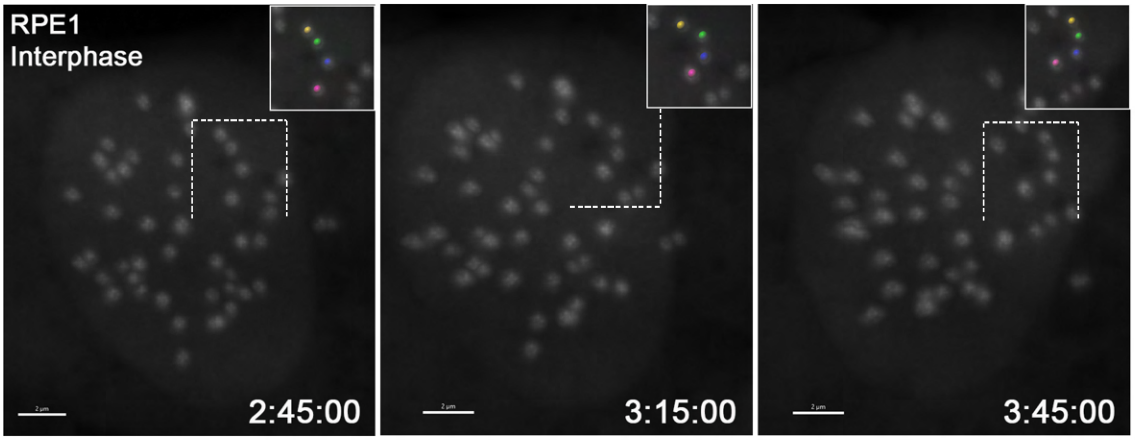

(Cai, Casas, Hua and Mikawa, Figure 4--figure supplement 1)

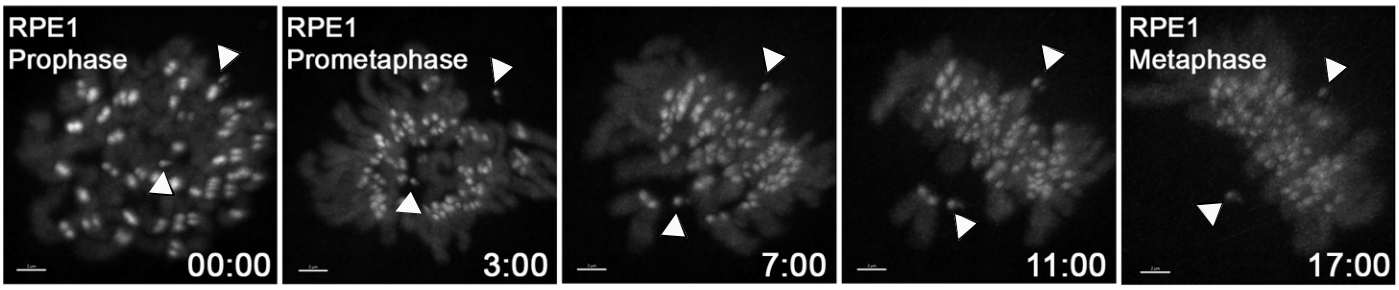

(Cai, Casas, Hua and Mikawa, Figure 5--figure supplement 1)